



Deposited via The University of Leeds.

White Rose Research Online URL for this paper:

<https://eprints.whiterose.ac.uk/id/eprint/98914/>

Version: Accepted Version

Article:

Christenson, HK and Thomson, NH (2016) The nature of the air-cleaved mica surface. *Surface Science Reports*, 71 (2). pp. 367-390. ISSN: 0167-5729

<https://doi.org/10.1016/j.surfrep.2016.03.001>

© 2016. This manuscript version is made available under the CC-BY-NC-ND 4.0 license
<http://creativecommons.org/licenses/by-nc-nd/4.0/>

Reuse

Items deposited in White Rose Research Online are protected by copyright, with all rights reserved unless indicated otherwise. They may be downloaded and/or printed for private study, or other acts as permitted by national copyright laws. The publisher or other rights holders may allow further reproduction and re-use of the full text version. This is indicated by the licence information on the White Rose Research Online record for the item.

Takedown

If you consider content in White Rose Research Online to be in breach of UK law, please notify us by emailing eprints@whiterose.ac.uk including the URL of the record and the reason for the withdrawal request.

THE NATURE OF THE AIR-CLEAVED MICA SURFACE

Hugo K. Christenson¹ and Neil H. Thomson^{1,2}

¹School of Physics and Astronomy, University of Leeds, Leeds LS2 9JT, U. K.

²School of Dentistry, University of Leeds, Leeds, LS2 9LU, U.K.

e-mail: h.k.christenson@leeds.ac.uk , n.h.thomson@leeds.ac.uk

Abstract

The accepted image of muscovite mica is that of an inert and atomically smooth surface, easily prepared by cleavage in an ambient atmosphere. Consequently, mica is extensively used a model substrate in many fundamental studies of surface phenomena and as a substrate for AFM imaging of biomolecules. In this review we present evidence from the literature that the above picture is not quite correct. The mica used in experimental work is almost invariably cleaved in laboratory air, where a reaction between the mica surface, atmospheric CO₂ and water occurs immediately after cleavage. The evidence suggests very strongly that as a result the mica surface becomes covered by up to one formula unit of K₂CO₃ per nm², which is mobile under humid conditions, and crystallizes under drier conditions. The properties of mica in air or water vapour cannot be fully understood without reference to the surface K₂CO₃, and many studies of the structure of adsorbed water on mica surfaces may need to be revisited. With this new insight, however, the air-cleaved mica should provide exciting opportunities to study phenomena such as two-dimensional ion diffusion, electrolyte effects on surface conductivity, and two-dimensional crystal nucleation.

Keywords: mica, muscovite mica, adsorption, potassium carbonate, water structure, capillary condensation, atomic force microscopy, surface forces

Contents

1. Introduction
2. The Crystal Structure of Muscovite Mica
3. The Surface Structure of Cleaved Mica and the Exchange of Surface Ions
4. The Cleavage Energy of Mica in Vacuum and in Air
5. Mica and the Surface Force Apparatus
6. Surface Analytical Studies of Air-cleaved and Vacuum-cleaved Mica Surfaces
7. Adsorption of Water Vapour to Mica Surfaces
8. Structure of Water Adsorbed to Mica Surfaces from Vapour
9. Adsorption of DNA to Mica
10. Epitaxial Crystal Growth on Mica
11. Origin of the Carbonate Ions on Mica
12. Concluding Remarks

Acknowledgements

References

1. Introduction

Muscovite mica is the substrate of choice for an ever increasing variety of experiments involving surfaces. Historically, studies of epitaxial crystal growth on mica go back at least to the first half of the nineteenth century [1; 2], and contact angle measurements of liquids on mica were also reported at a very early stage [3]. Gas and vapour adsorption work was carried out in the early twentieth century by Langmuir [4], and later Bangham and co-workers [5; 6], who also did wetting experiments [7]. Other early work focussed on the insulating properties of mica [8], and its use in capacitors and in quarter-wave plates. So widespread was the use of mica in electrical equipment that it was apparently referred to as “the most important single war material” during the Second World War [9]. One of the first studies to take advantage of the unique properties of muscovite mica is from 1930 and describes how the surface free energy of mica may be determined by measuring the force required to split a piece of mica along the basal plane [10]. Subsequently, the atomically flat nature of the mica surface was established by the work of Tolansky, who developed multiple-beam interferometry as a tool for studying the surfaces of crystals [11-13]. This led to the wide-spread use of mica for measuring frictional [14] and surface forces [15]. A summary of these early developments was given by Tabor [16].

Muscovite mica has been used for decades as a substrate for the preparation by vacuum evaporation of supporting carbon films for Transmission Electron Microscopy (TEM) [17]. It was adopted for use in Atomic Force Microscopy (AFM) soon after the invention of the technique, principally as a supporting surface for the study of molecular and nanoscale systems [18]. The atomic flatness of the (001) basal cleavage plane is the key reason for the use of mica in both these types of microscopy. The atomically flat nature of the mica surface has also led to its use as a template to create smooth surfaces of other materials, such as silver [19] or gold [20; 21]. Among other important properties are the high surface energy and

water wettability of mica, which ensure strong adsorption of molecules and other nanoscale objects in air or vapour. It has also been suggested that mica was involved in the origin of life on earth by acting as a selective adsorbent for nucleotides [22] or even a template for DNA [23; 24].

The focus of this review has its origin in some very early observations made with water condensed from vapour between mica surfaces in the Surface Force Apparatus (SFA) published in 1973 [25] by Israelachvili. Over subsequent decades it was slowly realised that the surface of muscovite mica that has been cleaved in an ambient atmosphere is very far from the inert and atomically smooth substrate that many, if not most, still assume. This emerged both from numerous experiments with the SFA, as well as from investigations of the mica surface with various surface analytical techniques. Taken together, these two separate and quite independent lines of investigation have led to the conclusion that a water-soluble potassium compound, most likely potassium carbonate, is present on air-cleaved mica surfaces. The extent to which this influences experiments with mica surfaces in vapour or in non-aqueous liquids is in some cases very clear, as when water condensed between mica surfaces exhibits the properties of a concentrated electrolyte solution. It is equally certain that the K_2CO_3 can have no effect on the properties of the mica surface after it is immersed in bulk water or aqueous solution, thereby dissolving the K_2CO_3 . In other cases, however, the possible effects are not easy to predict. In particular, the influence of the potassium carbonate on the results of many Scanning Probe Microscopy (SPM) studies of mica in vapour is not clear, and it may in some cases be necessary to revise the conclusions drawn from these experiments. Similarly, simulations or theoretical work based on an idealised surface of potassium ions randomly distributed over fixed sites on a molecularly smooth and regular, two-dimensional crystal lattice may not always be relevant to an air-cleaved mica surface.

We believe that the presence of potassium carbonate on air-cleaved mica surfaces has been proven beyond reasonable doubt, and it is in this spirit that this review has been written. It is nevertheless true that in the absence of a definitive chemical analysis showing its presence some shadow of a doubt must remain.

This review will begin by describing the bulk crystal structure of muscovite mica and the structure of the basal plane exposed on cleavage. Then, the possibility of exchange of the potassium ions that are distributed between the two surfaces on cleavage of the layered mica structure will be discussed. We will then describe experiments involving controlled cleavage of mica, which give a measure of the surface free energy and information on the manner in which the ions are distributed between the two surfaces, which in turn determines the surface charge that develops as the mica is cleaved. The use of mica in the Surface Force Apparatus and experiments which led to the discovery of the ionic compound on the surface will then be reviewed, followed by surface analytical investigations of the mica surface. Thereafter, we will give an overview of wetting and water vapour adsorption experiments, and recent work on the structure of water adsorbed from vapour on mica surfaces, with particular focus on scanning probe microscopy (SPM) experiments. We then discuss some work on DNA deposited from bulk solution and studied on the mica surface in humid atmospheres using AFM, which involves surface ions and also gives some information on the distribution of charge across the surface. Finally, we examine some cases where the potassium ions appear to be involved in epitaxial crystal growth on mica, and then touch on the possible mechanism behind the formation of potassium carbonate on cleavage of mica in air. We end by discussing ways in which experiments with air-cleaved mica surfaces may be adapted to become easier to interpret.

2. The Crystal Structure of Muscovite Mica

Muscovite mica is a layered phyllosilicate and hence a member of a group to which some of the most common minerals in the earth's crust belong, including clays such as montmorillonite, illite and kaolin. Linus Pauling first proposed the general structure of complex crystals such as the silicate minerals in the 1920s [26; 27], at the time when the first results of X-ray diffraction studies were becoming available [28]. The most abundant subgroup of phyllosilicates are the micas [29], which have a layered structure consisting of two tetrahedral sheets on either side of an octahedral sheet, and these 2:1 layers are bound together by interlayer cations (Figure 1a). The tetrahedral sheet consists of a honeycomb arrangement of hexagons of SiO_4 tetrahedra, where each tetrahedron shares three oxygens with the adjacent tetrahedra. Some of the SiO_4 tetrahedra are replaced by oxygen tetrahedrally co-ordinated around Al, less commonly Fe, or more rarely, Be, which gives rise to a net electron deficiency. The Al substitution is random (see Section 3) with the proviso that Löwenstein's avoidance rule forbids adjacent AlO_4 that are linked by one oxygen only [30]. The fourth oxygen in each tetrahedron points in a direction normal to the tetrahedral sheet, and forms part of the octahedral layer. Two oxygens from the tetrahedral layer, together with an unshared OH group lying below the centre of the SiO_4 hexagon of the tetrahedral layer (Figure 1b), form the three corners of the face of an octahedron parallel to the basal plane. At the centre of each octahedron is a cation, usually Al, Fe or Mg. The OH group may be partly or fully replaced by fluorine in some micas. Below the octahedral layer is a second tetrahedral layer, once again sharing two oxygens per tetrahedron. The stack of 2:1 layers is held together by interlayer cations situated between two SiO_4 hexagons on opposing surfaces. These interlayer cations compensate for the excess negative charge in the 2:1 layers that is caused by vacancies in the positions of the octahedral cations, dehydroxylation of the OH groups, or most commonly, by substitution either of trivalent

metals (usually Al or Fe) for Si in the tetrahedral positions, or of divalent metals for Al in the octahedral positions.

The micas are classified into trioctahedral, where all three octahedra in the smallest structural unit have cations at their centre, or dioctahedral, where there is a vacancy at the centre of every third octahedron. The valency of the interlayer cation allows for another level of classification; into true micas with a monovalent cation (usually Na⁺ or K⁺), or into brittle micas where the cation is divalent, most often Ca²⁺ or Mg²⁺. Both true and brittle mica can be either dioctahedral or trioctahedral. The interlayer cohesion is much larger for the brittle micas due to the greater charge of the cation, which leads to their characteristic brittleness, whereas the much lower interlayer cohesion of the true micas gives them their typical flexibility and ease of cleavage along the basal plane.

Muscovite mica is a dioctahedral true mica with the layer charge arising from a 1 in 4 substitution of Al for Si in the tetrahedral layer, and the 2:1 layers held together by K⁺. The unit cell of mica contains 4 formula units of composition KSi₃Al₃O₁₀(OH)₂ and the parameters of the monoclinic unit cell are a = 0.519 nm, b = 0.901 nm, c = 2.00 nm and β = 95.8° (Figure 1c). In the rest of this review we shall take the term “mica” to mean specifically “muscovite mica”. Since mica is a naturally occurring substance there are variations in the exact composition, and isomorphous replacements are common, most commonly Na for K, and Mg or Fe for octahedral Al. Over the years a number of refinements of the structure of muscovite mica have been made, and the crystallographic literature contains a number of detailed discussions of the structure of muscovite mica [27; 28; 31-33] most of which is of no concern for this review. It is, however, important to be aware of some of the instances where the structure of muscovite mica deviates from the ideal picture presented above. Similar but usually less pronounced structural distortions occur with other phyllosilicates.

In the octahedral layer only 2 out of 3 sites are occupied by an Al, and each empty site is surrounded by a hexagonal array of occupied sites. This causes a shift of the apical oxygens (the ones that are shared with the tetrahedral layer) towards the Al^{3+} and away from the empty octahedral sites, leading to a distortion of the hexagonal rings of apical oxygens. In order to reduce the strain associated with a misfit of an estimated 3-5% between the octahedral and tetrahedral layers adjacent SiO_4 tetrahedra are rotated in opposite directions, thereby bringing the basal oxygens closer to the octahedral sites. The result is that the hexagonal symmetry of the ideal SiO_4 ring is replaced by ditrigonal symmetry, where only alternate angles of the hexagon are equal (Figures 1c, 2a and 3). Finally, the SiO_4 tetrahedra must tilt so that the apical oxygens that form part of the octahedral layer adjust to the two longer edges of the distorted hexagons of apical oxygens. This leads to a shift of four of the six oxygens to form a puckered ring around each potassium ion. As a consequence of the hexagonal to trigonal change in symmetry, the amount of space available to the interlayer K^+ is reduced, which forces adjacent 2:1 layers apart by 0.06 nm so that the basal oxygen surfaces of opposing tetrahedral sheets are no longer in contact [31].

In the above we have ignored the structural diversity resulting from a stagger of the upper tetrahedral layer with respect to the lower tetrahedral layer adjacent to each octahedral layer. This results in structural variations known as polytypes which depend on the direction of stagger in the plane of the sheets [29; 34]. These are not of any consequence for the surface effects that this review is concerned with, and in any case muscovite mica is almost always of a polytype known as 2M_1 .

3. The Surface Structure of Cleaved Mica and the Exchange of Surface Ions

AFM is ideally suited to imaging very flat crystalline surfaces like mica down to atomic resolution, and the mica lattice is often used as an imaging standard for nanoscale calibration of the piezoelectric scanners in an AFM. Indeed, mica has been important as a resolution standard to aid understanding of AFM operation as well as in the development of AFM instrumentation [35-38]. A key challenge for AFM has been to achieve reproducibility, which requires good control of the interaction force between tip and sample, and is made difficult by the variable sharpness of commercial tips. Development of the instrumentation, imaging modalities and the force probes, however, has improved the quality and consistency of AFM data over the last two decades.

Early AFM studies of the mica surface employed contact mode where the tip is in continuous repulsive contact with the surface. This typically involves interaction between tens and hundreds of atoms, even if the AFM tip is atomically sharp, which yields atomic lattice resolution but may not give true atomic resolution. There are only a few AFM studies of mica cleaved and maintained in vacuum (UHV) and these investigated lateral forces and friction, and include Friction Force Microscopy (FFM) images involving stick-slip interactions, which gave insufficient resolution to distinguish the atomic lattice [39; 40]. The periodicity of the mica lattice can also be resolved in air by FFM [41; 42], and it is consistent with the expected unit cell dimensions of mica [43]. Sometimes, the very large attractive forces in air due to van der Waals and capillary interactions mean that significant damage can occur as the tip is dragged across the surface, resulting in a loss of lateral resolution. Indeed, by exerting forces >100 nN on mica using the AFM tip it is possible to mechanically wear through the 1 nm thick 2:1 layers between the K^+ ions, i.e. a half-unit cell c dimension at a time [44]. More detailed studies of wear on mica using a silicon AFM tip gave more insight into the process. Firstly, water plays an important role since physical damage in vacuum could not be achieved

up to loads of 400nN [45]. At high humidity (>70%), the presence of water reduces frictional forces [46] but can also lower the threshold load at which wear occurs [45]. This implies that water is involved in wear through an activated chemical process under the pressure of the AFM tip. Using contact mode atomic lattice imaging inside wear holes created on mica with the same tip, it was shown that wear can occur via the removal of just one layer of SiO₃ tetrahedral units, by removing half the unit cell, or a combination of both [45].

The best AFM images of the mica lattice are obtained in a liquid environment, where the long-range attractive Van der Waals interaction between tip and surface is significantly screened, enabling tip tracking of the surface with a smaller net force. Kuwahara has made perhaps the most detailed investigations of the mica lattice structure using contact mode under water with soft cantilevers of spring constant, $k \sim 0.1$ to 0.5 N/m [47; 48]. In this work he also reviewed images published in the 1990s and found that there were two basic image types that showed either, i) the hexagons of the silica tetrahedra that make up the basal plane, or ii) an hexagonal array of bright spots about 0.53nm apart, consistent with the a dimension of the unit cell [34] (Figures 2 and 3). The first category of image clearly looks like the hexagonal mica lattice close to atomic resolution. The second category has been proposed to arise from the detection of the K⁺ ions in the hexagonal cavities [49], although as Kuwahara pointed out, this is unlikely due to the ion exchange that often occurs upon immersion in aqueous solution (see below). Kuwahara found that the observation of one or the other of these cases appeared to depend on the direction of the cantilever long axis relative to the fast-scan direction [47]. Hence, a simpler interpretation is that with a change in the frictional force signal as the scan axis varies, the image changes from one depicting a hexagon of six basal plane oxygens surrounding a ditrigonal cavity, to one showing hexagonal arrays of three basal plane oxygens, where each triplet of oxygens appears as a bright spot [47] (Figure 3c).

Note, however, that a transition from one image type to the other may also occur without a change of scan direction [34].

Kuwahara based his conclusions on over 200 separate scans, and his study shows clearly the ditrigonal symmetry of the silica tetrahedra (Figures 2 and 3). Further analysis indicates that while tetrahedral rotation is responsible for the ditrigonal symmetry, the distance between hexagons also alters across the surface. This is a surface relaxation effect, due to additional tetrahedral rotation after cleavage since the K^+ are too large for their ditrigonal cavities in the bulk crystal, and of these cavities some increase in size while others must decrease in size after cleavage. The end result is that there is about a $\pm 5\%$ variation in the a and b unit cell dimensions across the cleaved mica surface. This work is strong evidence that AFM is capable of resolving finer details of the atomic structure, and Kuwahara also compared AFM images of muscovite and phlogopite (a magnesium-potassium aluminosilicate) surfaces with the bulk structure from X-ray diffraction [31] and found good agreement, although the surface relaxation with muscovite was more pronounced [48]. A more recent method called three-dimensional scanning force microscopy, which enables the 3D distribution of water molecules next to a surface to be visualised, has confirmed the surface relaxation of the ditrigonal oxygen rings in the basal plane [50].

More recent advances in AFM force control enable the tip-sample interaction volume under liquid to be reduced close to atomic dimensions, such that true atomic resolution is possible. Fukuma and co-workers have pioneered frequency modulation AFM (FM-AFM) and resolved atomic point defects in the mica surface under aqueous solutions [51]. Their FM-AFM studies also suggested that the AlO_4 in the tetrahedral layer could be distinguished from the SiO_4 because the lower charge of Al relative to Si makes these oxygens protrude slightly [52-54]. A recent X-ray study of mica [55] has provided detailed information on how the

surface relaxation of mica in aqueous solution subtly varies depending on the cation present next to the surface.

It has long been realised that aluminosilicates such as clays contain exchangeable ions between the platelets, and the K^+ on the surface of cleaved mica will also exchange with other cations present in solution. From the *a* and *b* lattice constants of mica, which contain two K^+ shared between two surfaces on cleavage, it follows that the average surface area per K^+ on the mica surface is 0.47 nm^2 . The first systematic studies of the ion-exchange properties of muscovite mica was carried out by Gaines [56]. He showed that only the K^+ on the exposed cleavage planes could be exchanged for other cations in solution, and that little or no penetration into the lattice occurred at moderate pH and immersion times of up to a few days. The K^+ on mica could be completely exchanged for hydrogen ions. Note that a recent study showing incomplete exchange was carried out with a system with a very limited reservoir [57]. A dynamic study of the surface potential after immersion of mica in water equilibrated with atmospheric CO_2 (pH 5.6) has shown that the K^+ have been essentially completely exchanged for H^+ after about 1 min [58].

XPS studies have shown that the surface K^+ on mica may be permanently exchanged for H^+ , Mg^{2+} and Ca^{2+} , but that Na^+ is washed off when rinsing the surface with pure water [59], although the Na^+ remain on the surface if acetone washing is employed instead [60]. It was also shown that the surface mobility of ions increased in the order $\text{H}^+ < K^+ < \text{Mg}^{2+}, \text{Ca}^{2+}$. When fully hydrated, the Mg^{2+} and Ca^{2+} are thought to be mobile across the surface but bind more strongly in limited water at low humidity [59]. A FFM study showed that atomic lattice resolution may be achieved on mica with H^+ and K^+ on the surface, but that with Mg^{2+} and Ca^{2+} this only occurs at higher humidity [61]. Friction signals in FFM arise from stick-slip adhesive interactions, so the study shows that the random positions of Mg^{2+} and Ca^{2+} after ion-exchange lead to a non-periodic stick-slip pattern at low humidities when the Mg^{2+} and

Ca^{2+} ions are immobile. At higher humidities the ions are easily displaced by the AFM tip to give the stick-slip traces of the underlying mica lattice.

The affinity of Li^+ and Na^+ for the mica surface is much less than that of K^+ [62] because their greater degree of hydration makes them unable to approach the surface close enough to fit into the ditrigonal cavities. By contrast, Cs^+ readily associates with the mica surface in solution [62]. The important point is that the interlayer K^+ left on the mica surface after cleavage exchange almost completely on immersion in water in equilibrium with the atmosphere. It is hence easy to prepare mica which has the surface K^+ replaced by H^+ (or H_3O^+), and in what follows we shall refer to such ion-exchanged mica as “H- mica”, and the untreated mica as “K- mica”. In many cases the ion-exchange has been carried out in 10^{-3} M HCl solution to drive the exchange reaction even further towards complete H^+ coverage of the mica surface [63; 64]. There have been suggestions that the H^+ may not reside in the ditrigonal cavities as H_3O^+ or other hydrated species, but that they bind either to oxygens in the basal plane, or penetrate the lattice and attach to the hydroxyl groups in the octahedral layer [60; 65].

The importance of the size of the surface ions relative to that of the ditrigonal cavities was shown by an investigation in which ion-exchanged mica with H^+ , Li^+ , and Mg^{2+} on the surface was heated to 300°C to completely eliminate water from the surface. Subsequent high-resolution AFM images showed Li^+ and Mg^{2+} in the hexagonal cavities, whereas such atomic-scale features were absent for H- and K-mica, suggesting that the former get irreversibly fixed into the cavities during dehydration. This study lent support to the idea that the ability of ions to bind into the ditrigonal cavities depends on their size and charge density, which is related to their enthalpy of hydration [66].

4. The Cleavage Energy of Mica in Vacuum and in Air

Because of its layered structure and the relatively weak attraction between the interlayer potassium ions and the negative charge of the tetrahedral layers mica is readily cleaved into thin layers. The resulting lamellae are very flexible and mica thus lends itself to the ideal experiment for measuring the surface free energy of a solid. The surface area can be increased continuously and in principle reversibly (by rehealing the crack), thus satisfying the criterion for a thermodynamic measurement – quasistatic and reversible. Such an experiment was first carried out by Obreimoff in 1930 [10], and has been revisited many times with muscovite mica [67-76] as well as phlogopite [67; 77]. It can be shown that the force required to prise the two layers of mica apart, times the distance over which this force is applied, is equal to the sum of the surface free energy of the two exposed surfaces and the elastic energy stored in the bent sheets [10]. When cleaving mica in air of unspecified humidity a value of 1.5 Jm^{-2} for the surface free energy γ was obtained by Obreimoff, who also reported that on recleaving the mica after rehealing the sheets a lower value was measured. If the splitting was carried out in a vacuum of 10^{-6} mm Hg, the measured γ was as large as 20 Jm^{-2} ! These very high values, as Obreimoff realised, were due to the force required to separate electric charges originating in the uneven distribution of potassium ions on the opposing surfaces after cleavage [78]. Metsik showed that the work required to cleave mica in air at $p = 0.1$ mm Hg depended on the rate of cleavage [72], with rates of 0.5 mm s^{-1} giving rise to free energies that oscillated wildly with time, increasing up to 15 Jm^{-2} and then falling as low as 1 Jm^{-2} , as electrical discharge across the gap between the surfaces occurred (Figure 4). At a slower cleavage rate of 0.05 mm s^{-1} the free energy varied between 3 and 4 Jm^{-2} only. Metsik also showed how to largely eliminate the effect of surface charge by conducting the cleavage experiments in nitrogen in the presence of an ionising source [72], which neutralised the surface charges and reduced the measured surface free energy to 960

mJm^{-2} . More recent work has shown that cleavage in dry nitrogen is also highly erratic and irreproducible due to the influence of the charge domains, with surface free energy values varying from 1 to 2 Jm^{-2} , but that a humidity of 5% or more is sufficient to largely eliminate the effect of charge domains on the surfaces [76].

When effects due to electrostatic charges are removed, direct cleavage experiments can provide information on how the surface free energy of the mica varies with adsorption from the atmosphere and on the crystallographic orientation of the two opposing mica surfaces. Bailey and Kay obtained 308 Jm^{-2} for mica cleaved for the first time in dry air (ca. 1 % relative humidity – r.h.), which decreased to 220 Jm^{-2} at a r.h. of 50-60 %, and 182.8 Jm^{-2} for r.h. > 90% [71]. If the mica was cleaved, subsequently resealed and then cleaved a second time, the surface free energy fell from 308 to 250 Jm^{-2} at 1% r.h., showing the effect of adsorption from the atmosphere. However, if the mica sheets were reoriented before resealing after cleavage at 50-60 % r.h., the decrease in surface free energy was much greater – from 220 to 120 Jm^{-2} , with the additional reduction of 100 Jm^{-2} due to the loss of lattice match on reorientation. More recent direct cleavage experiments in atmospheres of more accurately controlled humidity have qualitatively confirmed these results although higher values, particularly at low r.h. were obtained [76], with the surface free energy for virgin cleavage being very close to the 960 mJm^{-2} measured by Metsik [72].

It would be plausible to assume that the distribution of K^+ between the two surfaces on cleavage would be related to the distribution of oxygen tetrahedra in the surface layer that have aluminium atoms in their centre. The net negative charge of the AlO_4 would exert a greater attraction on the K^+ than the SiO_4 . While the exact degree of order of the aluminium substitution in the tetrahedral layer is unclear [31], there is evidence from Low-Energy Electron Diffraction (LEED) that the K^+ after cleavage are randomly distributed on each surface [78-80]. Notwithstanding the *locally* random arrangement of potassium ions, the

cleavage experiments show conclusively that domains of net charge are created on the surface on a larger scale. This can be visualised by decorating the freshly cleaved surface with charged particles, and the surface charge domains are found to be of the order of one mm^2 in size [68; 81; 82]. In an ambient atmosphere the charges are neutralised in a matter of minutes [67], and decay times of 2-8 minutes for surfaces at a r.h. of 30-48 % have recently been determined with AFM [83].

Campbell *et al.* studied freshly cleaved mica with AFM under ambient conditions (the exact humidity was not reported) and detected the presence of steps that were only about 0.1 nm high, and these steps were mobile and disappeared within minutes of cleavage [84]. Several possible mechanisms behind the occurrence of these steps were discussed, and the most likely candidate according to the authors was that the steps are the boundaries between higher, positively charged surface domains with K^+ in the ditrigonal cavities and lower, negatively charged domains with no ions. The authors further speculated that the disappearance of the charged domains could be related to an increased mobility of the K^+ as these became hydrated by adsorption of water from the atmosphere.

5. Mica and the Surface Force Apparatus

Muscovite mica was essential to the development of The Surface Force Apparatus, the SFA. This instrument grew out of a series of scientific developments in England during the middle of the twentieth century. Tolansky, at the University of Manchester, developed multiple-beam interferometry with silvered surfaces [11]. He used this refinement of the classical Fabry-Perot interferometer to study the surfaces and topography of crystals [13], and in particular used the technique to study the planes and cleavage steps on muscovite mica [12], noting that large, apparently molecularly smooth areas could be produced on cleavage, and

that the heights of the lattice steps were multiples of the unit cell dimension in the *c*-axis direction, i.e. 2.0 nm. Bailey and Courtney-Pratt at the University of Cambridge used multiple-beam interferometry of mica sheets sliding against each other in a crossed-cylinder configuration to study boundary lubrication [14]. The crossed-cylinder configuration was adopted by Tabor and Winterton, who designed the first surface force apparatus to use mica [15]. This was followed by further developments to the instrument [85], which eventually led to a number of similar devices designed primarily to measure surface forces between mica surfaces or mica substrates altered by various surface modification techniques across liquids [86-89].

Several factors make mica an unrivalled substrate for surface force measurements – it can be cleaved into macroscopic (cm²) sheets of constant thickness with atomically smooth surfaces. It is flexible, allowing it to be curved and mounted as crossed cylinders, which minimises alignment problems and allows an entirely new contact area to be obtained by shifting the surfaces in two orthogonal directions with respect to each other. Mica is transparent, permitting the use of multiple-beam interferometry, which has the advantage of allowing the refractive index of the medium between the surfaces to be determined and the occurrence of surface deformations or surface damage to be monitored. Mica is also comparatively inert, it is heat resistant with negligible changes to the surface up to ~450 °C [90], and it is unaffected by aqueous electrolyte solutions, dilute acids and alkalis as well as most organic liquids, apart from the likely exchange of the basal plane K⁺ if the liquid contains free cations.

Furthermore, the ion exchange properties of the mica surface allow for the facile preparation of, e.g. hydrophobic surfaces by replacing the K⁺ with cationic surfactants or lipids [91; 92]. Finally, by use of the Derjaguin approximation [93; 94] the force measured between crossed cylinders may be conveniently converted to the interaction free energy per unit area between

parallel, flat surfaces. This is often the most readily accessible quantity from theoretical models or computer simulations.

In the SFA, two back-silvered mica sheets are glued to cylindrically polished silica discs and then mounted facing each other in a crossed-cylinder configuration – equivalent to a sphere-on-a-flat (Figure 5a and b). The two back-silvered mica surfaces form a multiple-beam interferometer that will only transmit a series of discrete wavelengths of incident white light. These wavelengths depend on the surface separation and refractive index of the medium between the surfaces [13; 25], and by carrying out measurements with adjacent fringes of both odd and even order, one can determine independently both the surface separation and the refractive index. This feature makes the SFA particularly suitable for monitoring surface deformations and phase changes in the medium between the surfaces, such as condensation of liquid from vapour. One of the surfaces is mounted on a spring (a double-cantilever spring for optimum accuracy) and the separation between the mica surfaces is controlled by mechanical means using motors (with or without a differential spring system) and piezoelectric transducers. Surface forces are measured by calibrating the movement of the surfaces at large separations, in the absence of surface forces. Any force at smaller separations results in a deflection of the spring and hence a deviation in the movement of the surfaces, from which the force may be calculated using Hooke's law. If one wishes to minimise the spring deflection the lower surface is mounted on a very rigid support, such as the one illustrated in Figure 5b, which is useful for experiments where the forces are very large, such as those involving adhesion in vapour and capillary condensation.

Despite the inertness of mica, the first surface force experiments showed very clearly that changes occur at the mica surface on cleavage in laboratory air. With multiple-beam interferometry it could be established that the effective thickness of each mica sheet increases by 0.35 ± 0.1 nm when exposed to air of 50-80 % r.h. for 1 h [15], or about 0.32 ± 0.08 nm

when exposed to a r.h. of 40-45 % for 1 h [86]. In both cases, the authors concluded that a layer of the corresponding thickness adsorbs from air to freshly cleaved mica. In the latter study it was found that on subsequent immersion in water, the adsorbed layer appeared to dissolve, as the thickness of each mica sheet when brought into contact in water was the same as before exposure to air for 1 h. Mica is a high-energy surface, as shown by the direct cleavage experiments, and it is not surprising that adsorption of species from the atmosphere takes place. At the very least one might expect adsorption of water from the atmosphere at the humidities found during the above experiments. More surprising, perhaps, was that the adsorbed layer continued to increase in thickness with time, up to periods of several days, when its thickness reached 2-3 nm, and that it was found to have the very high refractive index of 1.8 ± 0.1 [86].

In more recent SFA experiments, the standard procedure has been to expose the mica to laboratory air only during cleavage of the mica and its subsequent gluing to supporting silica discs, giving a total exposure time of the order of half an hour or less (this can be significantly reduced by re-cleaving just before measurements as, mentioned in the discussion after eq. 4). Immediately thereafter, the surfaces are mounted in the SFA which is then purged with dry nitrogen. Under these conditions the subsequent contact in water is typically at some -0.3 nm with respect to contact between the mica surfaces in nitrogen (after the half-hour exposure to the ambient atmosphere) [95]. This suggests that air exposure only leads to a 0.1-0.2 nm increase in the average thickness of each mica sheet, but if any water remains trapped between the surfaces when in contact in water this could be slightly larger. Despite a very large body of experimental data, the SFA measurements alone have not definitively established how much water adsorbs to mica on cleavage in laboratory air, and whether or not any water remains between the surfaces when these are brought into contact in pure water.[95-97]

Some years previously, however, the abnormal behaviour of water that had condensed from vapour on mica surfaces was first reported [25]. Capillary condensates in the SFA show up as an annulus of liquid around the contact area of the flattened surfaces which turns into a liquid neck on separation of the surfaces that eventually evaporates and/or snaps – see Figure 5c. In this case the condensed “water” had a high refractive index (ca. 1.46) and did not evaporate as expected in an atmosphere undersaturated in water vapour. At the time the controversy surrounding anomalous water, or “polywater” was only just being settled [98] and the author chose not to elaborate further on the possible reasons for the unusual properties of these water condensates. Solute leaching from surfaces and dissolving in adsorbed films and capillary condensates had been shown to be responsible for numerous reports of “anomalous water” in the late 1960s and early 1970s [99; 100]. Although this had been found principally with silica and glass, other materials such as CaF₂ [101] and MgO [102] had also been implicated.

A few years later, the first experiments on capillary condensation of liquid between mica surfaces were carried out, and the Kelvin equation was for the first time accurately verified for capillary-held liquid, i.e. for negative radii of curvature of magnitude down to 5 nm [103]. The Kelvin equation describes the change in vapour pressure of a liquid due to interfacial curvature and is given by

$$RT \ln(p/p_0) = \frac{\gamma V_M}{r} \quad (1)$$

where p is the vapour pressure over a curved interface, p_0 is the vapour pressure over a flat interface (p/p_0 is hence equal to the relative vapour pressure or the relative humidity), γ is the interfacial (surface) tension, and r is total radius of curvature of the interface. The total radius r is given in terms of the two principal radii of curvature r_1, r_2 by

$$\frac{1}{r} = \frac{1}{r_1} + \frac{1}{r_2} \quad (2)$$

Agreement with the Kelvin equation was obtained with cyclohexane, but this could not be repeated with water, however, and this was attributed to the presence of carbonaceous, water-soluble material on the mica surfaces, which would remain as a solid residue on the surfaces after evaporation of the condensates. Since then, a great number of SFA experiments involving capillary condensation of nonaqueous liquids have been carried out [104-109], and not even with moderately polar liquids such as *tert*-butanol [110] or ethanol [111] has any contamination of the condensates been evident, which strongly suggests that the solute in the water condensates is ionic.

A significant difference in the adhesion behaviour of mica surfaces in water vapour and in cyclohexane vapour was also found [112]. Close to saturation, both for water and nonpolar liquids, the pull-off force F was found to be given by the negative Laplace pressure in a liquid capillary condensate, or

$$F = 4\pi R\gamma \cos \theta \quad (3)$$

where R is the radius of curvature of the mica surfaces and θ the contact angle of the liquid (water or cyclohexane) on the mica (so close to 0 that $\cos \theta$ can be assumed equal to 1). However, as p/p_0 decreased the pull-off force in cyclohexane stayed almost constant down to $p/p_0 \sim 0.1$, whereas with water there was a noticeable decrease already at $p/p_0 \sim 0.9$.

It was later shown that the main reason for the discrepancy was not related to the effect of a “carbonaceous layer”, but rather to the use of a single-cantilever spring for these measurements [113]. With such a spring, the surfaces move laterally and slide against each other as the remote end of the spring is shifted to separate the surfaces. If the friction between the surfaces is high they will come apart with a wrenching motion instead of

smoothly, and an anomalously low pull-off force is measured [114]. Since the adhesion between the surfaces is much larger in water vapour than in cyclohexane, the effect of the large friction at low relative vapour pressures (when there is less lubrication by adsorbed molecules [115]) has a greater effect on the apparent pull-off force in water vapour than in cyclohexane vapour. In more recent work with the SFA, a double-cantilever spring has become standard in order to avoid rolling and reduce sliding motion of the surfaces.

Quantitative data on the solute in water condensates between mica surfaces were first obtained during a series of experiments on the capillary condensation of water from nonpolar liquids, particularly from the silicone oil octamethylcyclotetrasiloxane (OMCTS) [116], which has been frequently used as a model liquid in SFA experiments [19; 116-120]. Capillary condensation of water from nonpolar liquids is thermodynamically analogous to condensation from vapour, and is described by a modified Kelvin equation (eq 1) in which the surface tension is replaced by the interfacial tension between water and nonpolar liquid, and the relative vapour pressure is replaced by the fractional water saturation of the nonpolar liquid. The refractive index of the water condensed between the mica surfaces was found to be higher than that of bulk water, but decreased towards the bulk value with increasing condensate size [116], consistent with an increasing dilution as the size of the condensate increased. Furthermore, the radius of curvature r of the condensate meniscus was inversely proportional to the logarithm of the water activity (concentration), as expected for a Kelvin-type equation, but the slope was about twice as large as expected (Figure 6). A solute in the capillary condensate would give an additional lowering of the vapour pressure of the water in addition to that caused by the interfacial curvature. The volume of the condensate varies as its radius squared [121], while the area in contact with the condensate is proportional to r [121], so if solute that is uniformly distributed over the two mica surfaces dissolves in the condensate, the concentration and the activity a_w for dilute solutions should decrease as $1/r$.

Since for a_w close to unity $\ln[a_w]$ is linearly proportional to a_w , $\ln[a_w]$ remains linear in $1/r$, as seen from Figure 5. This would be consistent with solute from the mica surface dissolving in the condensate.

The adhesion force between the mica surfaces was not measurably affected by the presence of solute in the condensates, but was within the experimental error of a few percent equal to that expected for pure water condensates. This is not surprising as ionic solutes have only a slight influence on surface and interfacial tensions. This investigation also showed that the water condensates form at finite separations as the surfaces are allowed to approach each other. It is the formation of this condensate that pulls the surfaces into contact, rather than the action of long-range van der Waals forces. In nonpolar liquids the distinction is easily made as the range of any attractive van der Waals force is much shorter, and the short-range interaction between the surfaces is often repulsive due to the presence of oscillatory solvation forces [118]. In air or vapour the separation at which capillary condensates form is often close to where an inward jump due to van der Waals forces is expected, or ca. 10-12 nm for substances where the adsorbed film thickness is 1-2 nm [89], and a detailed analysis is required to distinguish between the two mechanisms [111]. The mechanism of condensate formation for non-aqueous liquids was later shown to be consistent with a thickening of adsorbed layers induced by van der Waals forces between films on the opposing surfaces [105; 122]. We believe that thickening of adsorbed films appears more likely than the suggestion of Luna *et al.* - that water neck formation between the tip and sample surface in AFM takes place by condensation of water molecules from the atmosphere [123]. It seems unnecessary to invoke condensation of water from an undersaturated atmosphere when there is a reservoir of water in films adsorbed to the tip and sample surfaces. In the SFA experiments comparisons were also made between the formation of water condensates in OMCTS confined between K-mica and H-mica surfaces [124]. The

condensates were observed to form at slightly larger separations with the K-mica surfaces and it was suggested that this was due to a greater affinity of water for the potassium mica due to the surface K^+ .

In an effort to learn more about the nature of the solute in the condensates, experiments were carried out to condense water between two mica surfaces, separate these to rupture the condensate, and investigate any solid residue after evaporation of the same. After drying the surfaces over P_2O_5 for 3 days [125], carbon replicas, shadowed with Pt, were made of the surfaces and in transmission electron microscopy the presence of crystalline material on the surface was suggested by the obvious faceting of the deposits in a restricted area, possibly the location of the capillary condensate, but in addition there were ca. 25 nm wide, roughly cap-shaped particles uniformly distributed all over the mica surfaces, covering perhaps a few tenths of a percent of the area. Further experiments with mica samples that were simply air-cleaved and exposed to a humid atmosphere before drying them, showed that with drying times of up to 2 weeks larger, but more sparsely distributed crystals were found on the surfaces. The crystals had a clear, hexagonal morphology and were up to 0.5 μm in diameter, but quite flat. It seemed likely that the cap-shaped particles consisted of the same material that had with longer drying formed larger crystals.

If a mica substrate was ion-exchanged by dipping in dilute HCl (pH 3) to produce H-mica, no crystallites were found on the surfaces on subsequent drying. It was concluded that the K^+ were necessary for the formation of the crystals, and water and/or CO_2 from the atmosphere were suggested as a possible source of an anion. Such crystallites were later identified by AFM imaging of air-cleaved and dried mica surfaces [126], and it was eventually realised that exposure to humid conditions was not necessary, and cleavage of the mica at ambient humidity (40-50 %) was enough to give crystallites on drying. Examples of AFM images of such crystallites are shown in Figure 7.

In a series of measurements of the pull-off force between mica surfaces as a function of the relative vapour pressure of n-hexane, cyclohexane and water further information on the different behaviour of K-mica and H-mica was obtained [113]. For $p/p_s > 0.95$, near water-vapour saturation in the presence of a condensate of $r > 10$ nm, the pull-off force with H-mica was slightly larger than with K-mica, and there was a difference in the manner in which the surfaces came apart. With H-mica the surfaces separated abruptly from contact, whereas with K-mica the surfaces would move outwards by a few nm before jumping apart. This discrepancy is due to the different short-range force in water between mica covered mainly with H^+ ions and mica covered with mainly K^+ . With H-mica the short-range force is purely attractive, whereas with K-mica there is a short-range repulsion due to hydration of the K^+ [63; 64], which shifts the position of the outward jump by a few nm from contact.

A detailed study of the factors affecting the adhesion measured between mica surfaces in dry air/nitrogen and in water vapour led to several significant conclusions [95]. The initially measured pull-off force in nitrogen was high, and in good agreement with the results of direct cleavage experiments [74-76] and surface energies inferred from contact angle measurements [127]. According to the Johnson-Kendall-Roberts (JKR) theory [128] the experimentally determined pull-off force F is related to the surface free energy per unit area γ by the relation

$$F = 3\pi R\gamma \quad (4)$$

where R is the radius of curvature of the surfaces. JKR theory is expected to be valid for surfaces with large radii of curvature and large adhesion, which is the case for the mica surfaces used in the SFA [129]. The normalized pull-off force F/R decreased with time, from about $1.2 \pm 0.1 \text{ Nm}^{-1}$ (equivalent to a surface free energy of $\gamma \approx 0.13 \text{ Jm}^{-2}$) during the first few hours, to $0.9 \pm 0.1 \text{ Nm}^{-1}$ ($\gamma \approx 0.10 \text{ Jm}^{-2}$) after 24 h and $0.7 \pm 0.1 \text{ Nm}^{-1}$ ($\gamma \approx 0.07 \text{ Jm}^{-2}$) after 48 h, almost certainly due to the adsorption of contaminants from the gas phase. The adhesion

measured between H-mica surfaces was on average higher at about $1.4 \pm 0.1 \text{ Nm}^{-1}$ ($\gamma \approx 0.15 \text{ Jm}^{-2}$) during the first few hours. Similarly, direct cleavage experiments with resealed H-mica (the ion exchange was carried out after a first cleavage before resealing) showed no significant difference in the surface free energy compared to resealed K-mica surfaces [76]. In a later study, Frantz and Salmeron measured still higher values of the pull-off force between K-mica surfaces. By cleaving the mounted mica sheets in dry nitrogen immediately prior to the measurements using sticky tape [130], they obtained γ values of up to 0.30 Jm^{-2} for mica that had had very limited exposure to water vapour [131].

As a result of this detailed study of the adhesion between mica surfaces in air it was proposed that the anomalous properties of water condensed between mica surfaces was due to the dissolution of K_2CO_3 (or KHCO_3) in the condensates, and that the anions resulted from a reaction involving water vapour and CO_2 from the atmosphere [95]. It was concluded that the references to water-soluble organics that had often cropped up in connection with the adsorbed layer on mica were incorrect.

Finally, a study of capillary condensation of water with H-mica surfaces [132] was carried out and it showed that there was good agreement with the Kelvin equation in the absence of the potassium compound on the surfaces, and the refractive index of the condensed water was within error equal to that of bulk water (Figure 8b). Curiously, quantitative measurements of the size of water condensates between K-mica surfaces were only made much later [133] - the condensate size was not explicitly mentioned by Fisher and Israelachvili [103]. These data showed that the radii of curvature of the condensates on K-mica were about twice as large as expected from the Kelvin equation, a results that was very close to what had been found in the case of water condensing from OMCTS [116], discussed above (see Figure 8b). Moreover, the amount of potassium (as K_2CO_3) available on the mica surfaces in direct contact with the condensates was not sufficient to account for this

additional vapour-pressure lowering. It was inferred that the additional solute entered the condensates via diffusion along the surface, which is consistent with the diffusion that is necessary for the K_2CO_3 crystallites to form.

Measurements of the size of water condensates below 0 °C revealed that the interfacial radii of curvature of these supercooled condensates were only slightly larger than expected from theory (Figure 8a). At a temperature depression ΔT below the melting point T_m (of ice), water condensates at saturation are limited in size and their radius of curvature is given by a Gibbs-Thomson-type equation [134], or

$$r = \frac{\gamma V_M T_m}{\Delta H_{fus} \Delta T} \quad (5)$$

where ΔH_{fus} is the enthalpy of fusion. A reduction in temperature below T_m thus has the same effect as a reduction in vapour pressure below saturation above T_m . This has been found to accurately predict the size (proportional to the radius of curvature of the vapour-water interface) of condensates of cyclohexane [134] and neo-pentanol [108; 109] below T_m . With water, however, the condensate size and interfacial radius of curvature were larger than predicted, but good agreement was obtained by assuming that each water condensate contained all the K^+ (in the form of K_2CO_3) from the mica surface with which it was in contact. The vapour-pressure lowering due to potassium solute was then estimated to be one-fifth of that due to interfacial curvature. This suggested that the rate of surface diffusion of K_2CO_3 is significantly smaller at subzero temperatures, which is not unexpected [133]. Remarkably, it was found that the condensate sizes measured during the earlier study of capillary condensation from the nonpolar liquids OMCTS [116] were in almost quantitative agreement with those obtained for condensation from vapour (when adjusted for the difference between the interfacial tension between OMCTS and water and the surface tension of water, as required by eq. 1).

A number of experiments on capillary condensation of water between mica surfaces hence show that all the observed properties of the water condensates – the higher refractive index, the larger than expected interfacial radius of curvature, the negligible effect on the pull-off force and the crystalline residue left behind on evaporation and drying are consistent with the presence of a potassium salt in the condensates. If the K^+ are replaced by H^+ the properties of the condensates are consistent with those of pure water.

6. Surface Analytical Studies of Air-cleaved and Vacuum-cleaved Mica Surfaces

At the same time as SFA experiments were accumulating evidence for the presence of water-soluble material on the air-cleaved mica surface, several different surface analytical techniques were providing further support for this idea. Two years before the account of the non-evaporating capillary condensates was published, a study of the surface of cleaved mica with Auger spectroscopy [135] showed that the major surface contaminant on air-cleaved mica is a carbon compound that cannot be removed by heat treatment in UHV at 500 °C. However, long-term heating in an atmosphere of oxygen at 10^{-5} torr and 450-500 °C did remove the carbonaceous material, but also resulted in some loss of surface potassium. Furthermore, it was found that the carbonaceous material was present regardless of whether the mica was first cleaved in UHV and then exposed to air, or whether it was cleaved in ambient air from the start. Exposure of an UHV-cleaved mica surface to CO_2 , CO or CH_4 did not result in any carbonaceous surface layer, and it was suggested that the presence of water vapour was necessary for the formation of the carbonaceous material [135]. Clearly, all these observations are consistent with the presence of K_2CO_3 on air cleaved surfaces, but not with adsorption of hydrocarbons or other common organic contaminants which would not remain on the surface at 500 °C.

A comparison of the Auger spectra of vacuum-cleaved and air-cleaved mica, made in conjunction with an investigation of the adhesion between gold and mica, confirmed the presence of carbon or hydrocarbon impurities [82] on the air-cleaved surface. Furthermore, it suggested that the weak adhesion found between gold and air-cleaved mica is due to the presence of carbon or hydrocarbon impurities [82]. A comparison of the peak heights of the different spectra led the authors to suggest that the carbon-containing material was located between the K^+ , i.e. not covering them.

A later SSIMS (static secondary-ion mass spectrometry) study confirmed the presence of what was termed a “carbon compound” on the surface of air-cleaved mica [136], and that it could not be removed by subsequent exposure to UHV, and that it was absent on mica cleaved and maintained under UHV conditions. Additional SIMS studies comparing freshly cleaved and weathered mica surfaces showed that there was depletion of potassium from mica surfaces during weathering under ambient conditions [137], and that a corresponding increase in surface oxygen occurred. This is consistent with the formation and clustering of K_2CO_3 on the surface, since any aggregation of species would lead to a net reduction in average surface concentration when using a technique that probes only the outermost layers of atoms.

In an important contribution Bhattacharyya showed that CO_2 would adsorb on vacuum-cleaved mica, while air-cleaved mica showed no affinity towards CO_2 [138]. The author concluded that the lack of reactivity was due to the presence of a carbonaceous overlayer on the air-cleaved mica, the presence of which was confirmed in a later XPS (X-ray Photo Electron Spectroscopy) investigation [80]. Since the temperature-programmed desorption (TPD) of carbon dioxide in vacuum was found to follow second-order kinetics it was inferred that two surface species must be involved, at least one of which must be able to diffuse across the surface. The author considered it most likely that the mobile species would be a proton,

and that desorption would occur when it encountered a carbonate bound to a silicon in the top tetrahedral layer. Hence, the carbonaceous overlayer would originate when CO₂ binds to hydroxyl groups just below the oxygen hexagons of the mica surface to generate a bicarbonate species, which then releases a proton that can migrate along the surface and bind to a surface oxygen. These ideas will be further discussed in section 11.

Further evidence for the formation of a solid compound on the surface of mica came from a LEED investigation of air-cleaved mica that found evidence of nanostructures on the surface [139], which had not been noted in earlier studies [78]. Subsequently, while attempting to develop a method for contact printing of polymers and lipids with poly(dimethylsiloxane) (PDMS) stamps on mica, Workman and Manne found that patterns were produced even in the absence of lipid or polymer [140]. The patterns only appeared at intermediate humidities between 35% and 70% [140], and it was suggested that the patterns consisted of nanometre-thick layers of a potassium compound (assumed to be bicarbonate, not carbonate, although no evidence for this distinction was presented). Transport of surface potassium ions by adsorbed water was necessary for pattern formation, so the patterns were absent under dry conditions (<25 %) when not enough water was present, and at higher humidities (>70%), when the potassium compound remained dissolved in the water film.

Even stronger evidence for the presence of potassium carbonate on air-cleaved mica was obtained by Ostendorf *et al.* [141; 142]. Several previous studies [82; 135; 136; 138] were in agreement that the carbonaceous overlayer formed on cleaving mica in air could not be removed by exposure to UHV conditions. Ostendorf *et al.* carried out a comparative AFM study of mica cleaved in air and in UHV, and found very different results with the two samples of different origin [141]. The surface cleaved in UHV could not be satisfactorily imaged in non-contact mode due to the magnitude of the surface potential, typically between -80 and -130 V. The potential could not be reduced by annealing in UHV, even at 560 K, but

after a few minutes exposure to air the potential decreased to ± 2.5 V. The subsequent AFM images revealed the presence of numerous particles on the surface, of lateral size in the range 1-5 nm, and the authors suggested that these were the K_2CO_3 crystallites previously observed by one of us [125].

In a later study, the crystallites on air-cleaved mica samples were imaged at higher resolution by non-contact AFM in UHV [142]. Anhydrous K_2CO_3 , which normally forms at temperatures below 38 °C [143], is monoclinic with unit cell dimensions $a = 0.564$ nm, $b = 0.980$ nm, $c = 0.688$ nm and $\beta = 98.8^\circ$ [144], and high-resolution AFM scans showed row periodicities that were close to the a and b unit cell dimensions, indicating that the c -axis would be perpendicular to the surface. The angle of 117° measured between these rows is not, however, consistent with the bulk monoclinic structure of K_2CO_3 , which should give an angle of 90° , but rather suggests a hexagonal structure imposed by the underlying mica surface, as seems to be the case for the much larger crystallites imaged by AFM and shown in Figure 4 and also those published previously [125]. Potassium bicarbonate is also monoclinic but with very different lattice parameters ($a = 1.52$ nm, $b = 0.56$ nm and $c = 0.37$ nm, $\beta = 104.9^\circ$) [145] so this cannot explain the observations. The sesquihydrate of potassium carbonate is again monoclinic [146; 147], but its lattice parameters of $a = 1.19$ nm, $b = 1.38$ nm, $c = 0.71$ nm and $\beta = 120.6^\circ$ are not consistent with these AFM data [142]. It is very likely that the mica surface is able to impose a structure different from that of the bulk crystal with these very thin crystals that are only about 3 unit cells thick.

7. Adsorption of Water Vapour to Mica Surfaces

Langmuir [4] and later Bangham and Mosallam [5; 6] used muscovite mica as a substrate for vapour adsorption studies, but confined themselves to working with gases and organic liquids

and did not study adsorption from water vapour. Bangham and Saweris, however, investigated the spreading of various liquids on mica and found that water does not completely wet air-cleaved mica but has a finite contact angle (the value was not reported) [7], although for example methanol clearly wets mica, as shown by the interference colours around the edge of a spreading droplet. Complete wetting of a surface by a liquid is equivalent to that liquid spreading on the surface, or having a zero contact angle on the surface. Mica that has been cleaved in water vapour introduced into a previously evacuated chamber has been reported to be wetted by water [148; 149], and there is a very old observation of water having a zero contact angle on mica [3]. Salmeron quotes a value of 2.6° for the contact angle of water on mica exposed to air “for a couple of hours” [150], which is in agreement with our unpublished measurements on mica exposed for a few minutes only. However, a recent study reports a contact angle of only 0.06° for water around an air bubble pushed against a mica surface [151].

The adsorption isotherm of water on mica was measured with ellipsometry by Beaglehole *et al.* [152; 153], and the results showed a finite thickness of the adsorbed water layer at saturation (varying between 0.8 and 2.5 nm, depending on the mica samples used), in agreement with the small but finite contact angle observed experimentally. The finite film thickness and contact angle both contradict the results of the Lifshitz theory of van der Waals forces, which predicts that water should wet mica completely, i.e. a bulk water droplet should spread (contact angle = 0) and an adsorbed film of water should grow without bounds as saturation is approached [152; 153]. This disagreement is not surprising as Lifshitz theory is based on the dielectric properties of bulk materials, which will be very different from the dielectric properties of thin films where orientational effects such as those in hydrogen bonding are involved. Similar amounts of water adsorbed to mica [154; 155] were measured by Cantrell and Ewing using Fourier Transform Infrared (FTIR) spectroscopy, and they

found a limiting thickness of about 1.25 nm. A later multiple-beam interferometry study by Balmer *et al.* [156] only included measurements up to a relative vapour pressure of water of 0.9 (at which the adsorbed thickness was 0.6 nm), but the authors did investigate the effect of ion exchanging the surface. The adsorption isotherm of K-mica showed a more prominent knee at low pressures, but at relative vapour pressures in the range 0.5-0.9 the results were within error the same for surfaces with H⁺ or K⁺ (Figure 9). The average water layer thickness at $p/p_0 = 0.50$ was about 0.25 nm, so the influence of the K⁺ would appear to be unimportant for thicknesses above a statistical monolayer of water. Such a knee in the adsorption isotherm at low pressures is normally due to surface heterogeneities, i.e. sites with larger free energies of adsorption that lead to a greater increase of adsorption with vapour pressure at low pressures. The K⁺ on the surface are the obvious candidates for these sites, whether located in their ditrigonal cavities or elsewhere on the surface.

While the properties of mica as an electrical insulator are well known, adsorption of water from the atmosphere leads to a significant surface conductance at higher humidities. This is of importance to the use of mica in capacitors, as the increased surface conductivity leads to resistive losses [157-160]. It also means that mica in humid air can be imaged with Scanning Tunnelling Microscopy (STM) [161; 162], which requires conducting substrates. The surface conductance of mica increases approximately exponentially with the relative vapour pressure of water [161-163], and the mobility of K⁺ (as well as H⁺, Mg²⁺ and Ca²⁺) on mica also shows an exponential increase with relative humidity [59]. The surface conductivity of mica in water vapour has been said to be four orders [164] or five orders [161] of magnitude greater than if the layer were pure water, indicating the presence of considerable numbers of ions. The increase in conductivity with humidity can only be due to an increased mobility of these ions as it is difficult to understand why the number of ions would increase so drastically with the water vapour pressure. The presence of potassium ions on the surface accounts

qualitatively for this increase. At low humidity the K^+ , whether hydrated or not, are mostly present as scattered entities or as crystals of K_2CO_3 , depending on the previous history of the surfaces. Above about 42-43 % relative humidity (the vapour pressure over a saturated solution of K_2CO_3 [165]) the crystallites start to dissolve and the potassium ions, with any associated water become mobile, and this mobility increases with water content.

8. Structure of Water Adsorbed to Mica Surfaces from Vapour

The nature of the adsorption isotherm of water on mica provides some information on the structure of the adsorbed film, e.g. that the increased adsorption on K-mica compared to H-mica suggests that initially adsorbed water hydrates the potassium ions [156]. Additional information may be gleaned from studies of the temperature dependence of adsorption, which allows determination of the entropy and enthalpy of adsorption. Thus it was possible to conclude from the IR measurements discussed above [154] that water adsorbed to mica is more structured than bulk water, and that the first (statistical) layer of water in particular is highly ordered. A calorimetric study of water vapour adsorption to mica particles of diameter $< 5 \mu\text{m}$ and specific surface area $21.5 \text{ m}^2/\text{g}$ [166] confirmed that water at submonolayer coverages was more ordered than bulk water, but that the mobility of the water molecules increased at higher coverages. Detailed comparisons are difficult as a particulate sample contains different crystallographic planes at the edges of flakes in addition to the basal plane. Interestingly, the authors found that reversible migration of K^+ occurred in the presence of adsorbed water molecules.

The more detailed structure of adsorbed water films on mica has attracted considerable attention in recent years using various scanning probe techniques, X-ray reflectivity, surface spectroscopy as well as simulations. A difficulty when comparing the results of the different

studies is that some of these, experimental as well as simulations, strictly speaking deal with the interface between mica and bulk water [167; 168] whereas others consider a system of mica with a thin film of water in vapour [169-174]. These two systems may be quite different for films that are only a few water layers thick, when the mica-adsorbed film and the adsorbed film-vapour interface are not independent. We will concentrate on those studies that consider the mica in a vapour environment.

In AFM studies in ambient or controlled humidity environments a capillary neck of water forms between the surface and the tip at small separations (Figure 10), and this causes unwanted effects, such as a jump into contact [37; 123; 175-177], as occurs in the SFA (see section 5). In an AFM, however, these jumps are typically found to be an order of magnitude smaller, or of the order of 1 nm. The large attractive capillary interaction complicates contact-mode operation of AFM under ambient conditions by increasing the attractive tip-surface interaction and the frictional forces, and obviously makes the study of adsorbed water films impossible. This inspired the invention of amplitude modulated (AM) dynamic AFM modes with stiffer cantilevers than for contact mode operation, $k \sim 1$ to 50 N/m (compared to $k \sim 0.1$ to 0.5 N/m for contact mode) [178]. In a tapping-mode approach, the tip performs intermittent contact with the sample surface and the capillary neck is overcome periodically during the cantilever oscillation cycle of typically >10 nm. This method is robust but can limit the achievable resolution and may damage soft samples and sharp AFM tips. The physics of tapping mode in air is complicated by a bi-stable behaviour of the cantilever vibrating in the non-monotonic tip-sample potential, which can be further exacerbated by capillary neck formation between the tip and sample. For the underlying characteristics we refer the reader to the literature [179; 180]. Alternatively, the capillary interaction may be avoided altogether in a true non-contact (NC) mode experiment, where the water layers on tip and surface do not contact at all, by using a sufficiently small cantilever amplitude [123;

181]. The spatial resolution will be lowered somewhat because the tip is on average further away from the surface, but the dynamics of water films may be imaged reproducibly [181; 182]. Another method is to use a sufficiently sharp tip, where there is strong evidence that the capillary neck cannot form [183-185], as expected from restrictions imposed by the Young-Laplace equation as well as the tip size and geometry [183].

Before NC AFM in ambient conditions using AM control was established, a powerful derivative of AFM known as Scanning Polarization Force Microscopy (SPFM) (Figure 11) was introduced by Salmeron [186-189]. In SPFM a potential in the volt range (constant or of variable frequency) is applied between the metal-coated cantilever tip and the substrate. The potential induces an attractive force between the tip and the substrate, and this force is modified in the presence of adsorbed layers on the substrate. If the dielectric constant of the adsorbed layers is larger than that of the substrate, the attractive force between tip and sample increases and the force-feedback control compensates by moving the tip away from the surfaces. Consequently, adsorbed layers of a higher dielectric constant appear thicker, whereas those with a smaller dielectric constant than the substrate will seem thinner [188], but the absolute thickness of the adsorbed layers cannot be measured. In the case of mica in a humid environment, the polarization is sensitive to the orientation of adsorbed water molecules as well as the presence of mobile surface ions [59]. SPFM operates in non-contact mode due to the long-range nature of the electrostatic force between tip and sample and hence does not disturb adsorbed water or surface ions. Due to the larger tip-substrate separation compared to NC AFM the lateral resolution is limited to ca. 20 nm, but sub-micron size droplets of liquid on surfaces are nevertheless readily imaged [190; 191].

The results of SPFM studies of the mica surface suggested the presence of two distinct “phases” of water at low humidities. Below about 20% relative humidity a homogeneous water film designated phase I was found, whereas between 25 and 50 % r.h. a film of phase II

formed apparently hexagonal domains in epitaxial relationship with the mica substrate, and the authors suggested that it might be solid-like in nature (Figure 12a). Contacting the tip to the surface temporarily transferred adsorbed water to the tip, producing a depression in the surface film, which would disappear as water refilled the hole [187]. The time taken for the depression to refill varied with humidity and the structure of the film (phase I or phase II), and increased with the time of exposure to the ambient after cleavage.

In a later study the evolution of adsorbed water films was studied with SPFM after the films had initially been perturbed by contact with the tip [150]. It was found that the threshold humidity for the appearance of phase II correlated with that observed for the onset of capillary condensation during tip-sample contact. Once again the authors inferred the existence of a more strongly bound water layer at r.h. < 20 %, but now discussed the importance of the surface K^+ for phase II, present for $20\% < \text{r.h.} < 45\%$, although no evidence for solid residues of e.g., K_2CO_3 after drying was found [150].

Experiments using sum-frequency generation vibrational spectroscopy provided further evidence of a solid, ice-like water structure on mica, with no free (dangling) hydrogen bonds [192]. Together with the repeat measurements using SPFM a slightly revised picture of the structure of water layers on mica was obtained, with a very low water coverage below 20% humidity and a gradual increase in water with ice-like, ordered structure until full monolayer coverage was reached at ca. 90 % humidity [192]. In a subsequent study the humidity was increased beyond 90%, and it was found that water films with dangling H-bonds appeared at room temperature, but that in adsorbed films below 0 °C the ordering without free H-bonds persisted to larger thicknesses, leading to a ferroelectric structure of the adsorbed film [193] (Figure 12b).

In agreement with the results of Salmeron, a molecular dynamics simulation of water adsorbed to mica from vapour found that water condensed into a completely connected, two-

dimensional network of hydrogen bonds at monolayer coverage [172], designated 2D-ice by the authors. Although the simulation cell covered only two unit cells of the mica surface, establishment of this hydrogen-bond network appeared to be more important than solvation of the potassium ions. More recent simulations, however, have contradicted this picture and found little indication of well-ordered, 2-dimensional ice-like structures [174], and concluded that the water adsorption is influenced both by H-bonding to surface oxygens and hydration of potassium ions. A grand canonical Monte Carlo simulation of the adsorption isotherm of water on mica [170] was able to reproduce accurately several features found in the experimental adsorption isotherm by Balmer *et al.* [156]. It was found that initial adsorption for $p/p_0 < 0.1$ occurred both into the plane with the K^+ (i.e. between the K^+) as well as into a second layer hydrating the K^+ , resulting in a knee as observed experimentally. There was no indication of ice-like structures in the adsorbed film, which showed considerable heterogeneity because the water was strongly bound both to the K^+ and the basal plane oxygens. The authors also found that the results were consistent with the experimentally observed (most commonly) partial wetting of mica by water. A density-functional study of water on the mica basal plane has concluded that the properties of water adsorbed on mica are dominated by hydration of the K^+ rather than ice-like coordination of water with the basal oxygens [173].

Nevertheless, a relatively recent imaging study by AFM has claimed to resolve ice-like ordering of water on mica in humid environments [194]. Although interpretation of these images has similar issues to those of the mica lattice under liquid, the group used force measurements in combination with imaging to corroborate their findings. The same group has also reported that it is possible to use the AFM tip to write nanochannels into the ice-like layer at humidities above 30%, with long relaxation time-scales of a tenth of a second [195]. Other force measurements between a tungsten tip and mica detected a short range (~ 0.5 nm)

repulsive force before contact which was also attributed to an ice-like water layer [196]. The onset of these forces corresponded to 20% humidity, which correlates with the onset of capillary condensation and the transition between phase I and phase II water as described by the Salmeron group. Furthermore, Monte Carlo simulations of water films on mica by Meleshyn [169; 171] found support for the existence of polygonal water islands on mica as observed with SFPM, and attributed them to clusters of K^+ with a saturated first hydration shell.

Developments in the reconstruction of tip-sample forces from amplitude-distance measurements, both in the large and small amplitude limits [197-200], have enabled AM AFM measurements of the thickness of thin water films, which on mica [201] appear to be consistent with the results of other techniques [152-154; 156], and also show the importance of ageing or weathering effects [201].

9. Adsorption of DNA to Mica

The use of mica as a substrate for the study of biomolecules with AFM was mentioned in the Introduction. In most cases the studies are carried out in aqueous solution where the K^+ will have been exchanged for other ions. There are some examples, however, where the measurements are performed in humid atmospheres, involving in particular DNA, and these provide interesting information on some properties of mica relevant to the subject of this review.

Hansma and Laney showed [66] that linear, double-stranded (ds) DNA would bind tightly enough to mica for tapping mode AFM imaging in solution in the presence of divalent transition metal ions. The strength of the binding correlated with the cationic radius, which is approximately inversely proportional to the enthalpy of hydration, so the authors concluded

that it was related to how well the cations would fit into the ditrigonal cavities. The strongest binding was found with Ni^{2+} , Co^{2+} and Zn^{2+} , whereas Mg^{2+} would not bind DNA tightly enough for imaging. A flow-through system that enabled the adhesion of DNA to mica to be switched on and off was devised for solutions containing Zn^{2+} [202].

Rivetti and Bustamante deposited linear dsDNA on mica from solutions containing different cations, imaged the surfaces in air and then analysed the shape of the DNA molecules using polymer-chain statistics [203]. The results indicated that when the mica was treated with Mg^{2+} the DNA molecules could diffuse across the surface and find their lowest energy configuration in 2D (Figure 13b). In the absence of Mg^{2+} the DNA coils could overlap if sufficiently long, indicating a different mechanism of binding to the surface. This case is known as kinetic trapping, where the DNA backbone is pinned at the points of contact with the mica and the conformation is a projection of the 3D solution conformation onto the 2D mica surface (Figure 13c). In bulk, mica treated with Ni^{2+} usually gives rise to kinetic trapping with long DNA strands [204].

Billingsley *et al.* found that sufficiently short dsDNA molecules (< 800 base pairs, or 260 nm long) deviated from the expected average binding conformation on Ni-mica [205]. These molecules were characterised by surface-equilibrated conformations rather than being kinetically trapped, which provided evidence that the surface distribution of Ni^{2+} on the mica was not homogeneous. A model involving patches of charge on the mica surface was proposed, where the effective size of the Ni^{2+} -binding domains was of the order of ~100nm across (Figure 13a). This suggests that when mica is cleaved it may have electrostatic domains at the nanoscale as well as on the aforementioned longer length scales [68; 81; 82], and that these domains somehow persist for long enough to influence the ion-exchange procedure. In these AFM experiments the time between cleavage and ion-exchange was of the order of seconds.

The ionic “patchiness” of mica at the nanoscale was supported by the results of an earlier humidity controlled AFM study on Mg-mica and Ni-mica using 3 different topologies of circular DNA (plasmids) [206]. At sufficiently high humidity (>90%) where the water layer thickness on mica approaches the dsDNA diameter of 2 nm, irreversible conformational switches were observed in DNA molecules containing supercoiling strain energy. The change was greatest on Ni-mica for supercoiled plasmids: the implication being that the partial 3D conformation of these molecules means that they are not fully bound to the surface and able to re-arrange.

Mica in a humid atmosphere with double-stranded DNA bound to the surface with Ni^{2+} was studied by AFM imaging in NC mode [207]. The well-defined diameter of the dsDNA molecule could be used as a “molecular dip stick” since the apparent height of the molecule is influenced by the adsorbed water thickness surrounding the DNA [208]. The kinetics of water layer formation were influenced by the incubation time of the mica in Ni^{2+} solution (30 s or 5 min) as well as the time the Ni-mica was left at ambient humidity (hours to days).

It is clear from these AFM studies and those mentioned in section 3 that the process of ion-exchange of K^+ at the surface of mica is a complex process. DNA binding to mica appears to require the presence of divalent cations and their ability to bind into the ditrigonal cavities depends on their hydration. The DNA conformations give additional evidence of the mobility of certain ions on the surface (i.e. equilibration vs kinetic trapping) and while the K^+ ions are not directly implicated in DNA binding, the persistence of charged domains on the surface suggests that they play a role in the ion-exchange process.

10. Epitaxial Crystal Growth on Mica

The use of mica in early studies of epitaxial crystal growth [1; 2] was mentioned in the Introduction, and numerous investigations of epitaxy of especially alkali halides on mica have since been carried out, using both vapour deposition [209] and solution growth of crystals [65; 210-212]. The utility of mica for studying epitaxy is obvious; the basal plane exposed on cleavage provides large, atomically smooth surfaces with a regular crystal lattice. Of particular interest for this review, however are some cases where the presence or absence of potassium ions appears to have a major effect on crystal growth and epitaxy on the mica surface. For example, Christenson and co-workers have found an intriguing difference between freshly cleaved and slightly “weathered” mica in a study of CaCO_3 precipitation on mica from aqueous solution [213]. Calcite does not grow epitaxially on freshly cleaved mica, but if the mica has been exposed to a low-humidity (< 40-45%) environment for 30 min or more after cleavage the calcite crystals will grow preferentially oriented with the *c*-axis perpendicular to the mica basal plane (Figure 14). No epitaxy is found if the mica has been exposed to very humid atmospheres (> ca. 70%) at any stage before immersion in solution. Epitaxy only occurs if the mica is immersed directly in a metastable solution of Na_2CO_3 and CaCl_2 , not if it is first immersed in one of the two solutions before the second one is added. There is no epitaxy with H-mica. It appears as if K_2CO_3 must be present on the surface at the moment of contact with the metastable solution to induce epitaxy, but the mechanism behind this is not clear. Perhaps a local and transient increase in carbonate ion concentration contributes. However, calcite also grows epitaxially on both freshly cleaved and weathered surfaces of the related phyllosilicates lepidolite, biotite and vermiculite [214]. The interlayer cation of the first two is K^+ , as for muscovite mica, but in vermiculite the interlayer cation is Mg^{2+} . There is clearly scope for more work on this topic.

Tungsten oxide (WO_3) is a wide-gap semiconductor with important applications in nanoscale electronics. Nanowires of tungsten oxide may be grown on mica by subliming a WO_3 thin film onto the substrate at atmospheric pressure, 30-40 % relative humidity and the relatively low temperature of 550 °C [215]. This temperature is far below the sublimation temperature of bulk WO_3 , and it is likely that water vapour is involved by converting the oxide to a hydroxide. The nanorods are epitaxially oriented by the mica surface and grow at angles that are multiples of 60°, as expected from the pseudohexagonal surface lattice of the mica (Figure 16). Similar nanorods do not form on surfaces such as Al_2O_3 or SiO_2 , and it has been shown that the K^+ from the mica surface are involved by forming a non-stoichiometric tungsten bronze K_xWO_3 as an intermediate [215; 216]. Subsequently, it was demonstrated that only freshly cleaved mica produced the optimum conditions for nanorod growth [217]. Mica that had been annealed for 10 min at 350 °C and mica that had been kept for 10 min in ambient air gave a significantly reduced density of oriented nanorods, or none at all, and also showed a depletion of surface K^+ according to XPS measurements. As the authors concluded, these observations are consistent with the potassium ions of the mica surface very quickly becoming locked up in K_2CO_3 crystallites and hence not as readily available for the formation of the tungsten bronze, which is necessary for the growth of the oriented nanorods [217]. When the K^+ collect in crystallites the mean surface density as measured by XPS would decrease as the signal from some of the deeper lying K^+ will be shielded by those above.

Another example of the influence of the potassium ions on crystal growth involves vapour deposition of pentacene on mica [218], during which high-aspect ratio nanorods grow oriented parallel to the surface. However, if the potassium ions are removed by rinsing with water or acetone, or the surface is intentionally contaminated with diffusion pump oil, the crystals take on a different orientation perpendicular to the surface. The crystal growth of a

second rod-shaped aromatic molecule, para-hexaphenyl, has also been shown to be sensitive to the presence of K^+ on the mica surface [219]. With freshly air cleaved mica the vacuum-deposited para-hexaphenyl formed flat, needle-shaped crystals lying on the surface, whereas if additional potassium was vacuum-deposited on the mica surface, the crystals adopted a standing configuration. The authors explained the difference by assuming that the additional potassium disrupted lateral electric fields present on the air-cleaved mica.

It is likely that there are many more examples of crystal growth and orientation being influenced by the surface potassium, although the mechanism behind this may be unclear [220; 221]. There is call for more extensive studies of such cases since it is a relatively simple matter to exchange the potassium for hydrogen ions or other cations.

11. Origin of the Carbonate Ions on Mica

The carbonate ions on the air-cleaved mica surface must result from some reaction between atmospheric carbon dioxide and water catalysed by the mica surface. That this might occur is perhaps not entirely unexpected as zeolites, which are well known for their catalytic properties, are aluminosilicates like mica. The possible mechanism of this catalytic surface reaction appears to have been first discussed by Bhattacharyya [138], whose postulated mechanism for CO_2 adsorption and conversion to a carbonate species at the mica surface was mentioned in section 6. The hypothesis was that CO_2 would attack a hydroxyl site in the outermost tetrahedral layer to form a bicarbonate species, which would then dissociate into a carbonate and a proton that would migrate along the surface until it became stabilised near an aluminium site. Our extension of this idea would be that this H^+ replaces the K^+ in neutralising the lattice charge, and that two K^+ together with the carbonate then form K_2CO_3 , which becomes mobile on the surface in the presence of water, but crystallises under

dry conditions. However, we do not feel that we are in a position to speculate on the details of the mechanism, or exactly where the H^+ might reside.

The general idea is based on earlier work showing the presence of carbonate species after adsorption of CO_2 on zeolites [222]. Zeolites and mica are both aluminosilicates and are hence chemically closely related, but with an important structural difference. Zeolites are porous on the nanoscale and able to absorb large amounts of gases and small molecules in the pores. Zeolites are potent catalysts with numerous industrial applications and there is currently considerable interest in the use of zeolites for the separation and capture of CO_2 from industrial emissions [223]. Further examples of carbonate formation in zeolites are to be found in the more recent literature [224-227], and there have even been cases of carbonate species forming on the external surfaces of the nanoporous zeolites [228].

In the case of zeolites an increase in the amount of AlO_4 compared to SiO_4 favours adsorption of CO_2 because of the resultant increase in surface charge [223]. Compared to zeolites, mica has a very large AlO_4 to SiO_4 ratio, so CO_2 adsorption should be favoured, as should the initial presence of K^+ on the surface. Indeed, the mesoporous aluminosilicate Al-SBA-15 doped with K^+ shows greater CO_2 adsorption than when doped with Li^+ , Na^+ or Cs^+ [229]. Proton migration such as that envisaged to accompany carbon dioxide binding to the mica surface is an important elementary step in the catalytic activity of zeolites [230]. Finally, it should be noted that similar reactions that lead to the formation of carbonate species occur on many other mineral surfaces, e.g. alumina [231], and iron oxide [232] and ceria [233], in the last case even on macroscopically flat surfaces.

Although the details of the reaction leading to the formation of potassium carbonate on the mica are yet to be clarified there is overwhelming direct evidence for the presence of potassium carbonate on the surface shortly after cleavage in air, and its formation is entirely consistent with the properties and behaviour of structurally very similar aluminosilicates.

12. Concluding Remarks

The existing literature provides a wealth of evidence that muscovite mica cleaved in laboratory air bears a water-soluble compound which is almost certainly anhydrous potassium carbonate. Using the bulk density of 2430 kgm^{-3} and the surface area per K^+ of 0.47 nm^2 this is equivalent to a 0.10 nm thick layer of K_2CO_3 covering the entire surface. This amount is consistent with what would be contained in the 25 nm wide, cap-shaped K_2CO_3 particles covering perhaps a few tenths of a percent of the surface area of the mica [125], which were discussed in section 5. This surface density of K_2CO_3 is also consistent with the amount dissolved in the subzero water condensates mentioned in the same section [133].

On formation of K_2CO_3 after cleavage, perhaps according to a mechanism similar to the one suggested by Bhattacharyya [138] (section 6), the K^+ neutralising the lattice charge would be replaced by H^+ . Strictly speaking, this then means that the main function of the ion exchange procedure used in the SFA experiments is to wash the K_2CO_3 from the surface, rather than replace any ions neutralising the lattice charge of the mica. We do not know, of course, how quickly after cleavage all the carbonate ions form, and whether or there is only partial conversion. The amount of epitaxy of calcite apparently induced by K_2CO_3 [213] does depend on time, but this is most likely related to surface transport of material rather than to a reaction rate.

The implications of the K_2CO_3 for water condensed between mica surfaces in reasonably large volumes, such as the capillary condensates discussed earlier, is clear. However, the effect on adsorbed water films of nm-size thickness is less obvious. There is currently some theoretical disagreement about the relative importance of water adsorption to the tetrahedral oxygens in the mica basal plane on the one hand, and hydration of the potassium ions on the other [170; 172-174]. Resolving this controversy by experimental means will be difficult

unless proper account is taken of the K_2CO_3 on the surface. To carry out experiments with H-mica is straightforward – all it takes is a quick dip in a weakly acidic solution - but very few examples are to be found in the literature [234]. Similarly, few other authors have discussed the implications of the K_2CO_3 for their work [140; 150; 201; 217]. It is possible that the only way in which to ensure that the mica has K^+ in the ditrigonal cavities rather than dispersed across the surface as K_2CO_3 , is to ion-exchange the mica in an aqueous solution with K^+ at a high enough pH to avoid any H^+ adsorption. There are examples of work where it is difficult to believe that the presence of K_2CO_3 on the surface is not playing an important role in the observed behaviour of the system [22; 40; 235-237]. Simulations in which the K^+ are placed in ditrigonal cavities may not always provide the best model for the behaviour of air-cleaved mica [169; 171; 172; 238]. There has recently been great interest in studying mica coated with graphene sheets [239-241], e.g. for trapping nanosize water droplets between the mica and graphene, and here, too the likely presence of K_2CO_3 on the surface may need to be taken into account.

Although the presence of mobile K^+ and CO_3^{2-} on the air-cleaved mica surface undoubtedly complicates the interpretation of many experiments and makes comparisons with simulations and theory less straightforward, it may have some potentially useful consequences. The layer of K_2CO_3 may to provide an interesting model system for the study of two-dimensional ion diffusion and electrical conductivity. Such studies could be carried out as a function of both temperature and humidity.

Acknowledgements

We thank M. M. Kohonen, N. Maeda and D. Nowak for providing images for Figures 7 and 14, and I. Matolinova for supplying us with the original image for Figure 15. HKC

acknowledges financial support from the EPSRC (EP/M003027/1), useful discussions with M. M. Kohonen over the years, and J. M. Campbell is thanked for a critical reading of the manuscript.

References

- [1] M.L. Frankenheim, *Annalen der Physik* 37 (1836) 516-522.
- [2] M. Royer, *C. R. Acad. Sci.* 191 (1930) 1346-1348.
- [3] G. Quincke, *Annalen der Physik Neue Folge* (1877) 10-194.
- [4] I. Langmuir, *J. Am. Chem. Soc.* 40 (1918) 1361-1403.
- [5] D.H. Bangham, S. Mosallam, *Proc. R. Soc. (London) A* 166 (1938) 552-568.
- [6] D.H. Bangham, S. Mosallam, *Proc. R. Soc. (London) A* 165 (1938) 558-571.
- [7] D.H. Bangham, Z. Saweris, *Trans. Faraday. Soc.* (1937) 554-570.
- [8] O.N. Rood, *Am. J. Sci.* 14 (1902) 161-165.
- [9] Anonymous, *Nature* 157 (1946) 849-850.
- [10] J.W. Obreimoff, *Proc. R. Soc. (London) A* 127 (1930) 290-297.
- [11] S. Tolansky, *Nature* 152 (1943) 722-723.
- [12] S. Tolansky, *Proc. R. Soc. (London) A* 186 (1946) 261-271.
- [13] S. Tolansky, *Multiple-Beam Interferometry of Surfaces and Films*, Clarendon, Oxford, 1948.
- [14] A.I. Bailey, J.S. Courtney-Pratt, *Proc. R. Soc. (London) A* 227 (1950) 500-515.
- [15] D. Tabor, R.H.S. Winterton, *Proc. R. Soc. (London) A* 312 (1969) 435-450.
- [16] D. Tabor, *Colloids Surf.* 65 (1992) ix-xiii.
- [17] M. Spencer, *J. Biophys. Biochem. Cytol.* 6 (1959) 125-126.
- [18] B. Drake, C.B. Prater, A.L. Weisenhorn, S.A. Gould, T.R. Albrecht, C.F. Quate, D.S. Cannell, H.G. Hansma, P.K. Hansma, *Science* 243 (1989) 1586-1589.
- [19] J.L. Parker, H.K. Christenson, *J. Chem. Phys.* (1988) 8013-8014.
- [20] H.J. Butt, D.N. Wang, P.K. Hansma, W. Kuhlbrandt, *Ultramicroscopy* 36 (1991) 307-318.
- [21] N.H. Thomson, B.L. Smith, N. Almqvist, L. Schmitt, M. Kashlev, E.T. Kool, P.K. Hansma, *Biophys. J.* 76 (1999) 1024-1033.
- [22] G.L. Gaines, *J. Colloid Interface Sci.* 34 (1970) 326.
- [23] H.G. Hansma, in: N. Tamura, A. Minor, C. Murray, L. Friedman (Eds.), *Probing Mechanics at Nanoscale Dimensions*, Materials Research Society, Warrendale, 2009, pp. 105-110.
- [24] H.G. Hansma, *J. Theor. Biol.* 266 (2010) 175-188.
- [25] J.N. Israelachvili, *J. Colloid Interface Sci.* 44 (1973) 259-272.
- [26] L. Pauling, *J. Am. Chem. Soc.* 51 (1929) 1010-1026.
- [27] L. Pauling, *Proc. Nat. Acad. Sci. (USA)* 16 (1930) 123-129.
- [28] M.C. Mauguin, *C. R. Acad. Sci.* 186 (1928) 879-881.
- [29] S.W. Bailey, *Micas*, Mineralogical Society of America, Washington D. C., 1984.
- [30] W. Lowenstein, *Am. Mineral.* 39 (1954) 92-96.
- [31] E.W. Radoslovich, *Acta Cryst.* 13 (1960) 919-932.
- [32] N. Güven, *Z. Kristallogr.* 134 (1971) 196-212.
- [33] C.A.J. Appelo, *Am. Mineral.* 63 (1978) 782-792.

- [34] R.V. Coleman, Q. Xue, Y. Gong, *Surf. Sci.* 297 (1993) 359-370.
- [35] B. Drake, C.B. Prater, A.L. Weisenhorn, S.A.C. Gould, T.R. Albrecht, C.F. Quate, D.S. Cannell, H.G. Hansma, P.K. Hansma, *Science* 243 (1989) 1586-1589.
- [36] H. Hartman, G. Sposito, A. Yang, S. Manne, S.A.C. Gould, P.K. Hansma, *Clays and Clay Minerals* 38 (1990) 337-342.
- [37] T.G. Sharp, P.I. Oden, P.R. Buseck, *Surf. Sci. Lett.* 284 (1993) L405-L410.
- [38] Y. Seo, H. Choe, W. Jhe, *Appl. Phys. Lett.* 83 (2003) 1860-1862.
- [39] R.W. Carpick, N. Agrait, D.F. Ogletree, M. Salmeron, *Langmuir* 12 (1996) 3334-3340.
- [40] R.W. Carpick, N. Agrait, D.F. Ogletree, M. Salmeron, *J. Vac. Sci. Technol. B* 14 (1996) 1289-1295.
- [41] O. Marti, J. Colchero, J. Mlynek, *Nanotechnol.* 1 (1990) 141-144.
- [42] R. Erlandsson, G. Hadziioannou, C.M. Mate, G.M. McClelland, S. Chiang, *J. Chem. Phys.* 89 (1988) 5190-5193.
- [43] Z.H. Liu, N.M.D. Brown, *J. Phys. D: Appl. Phys.* 30 (1997) 2503-2508.
- [44] S. Miyake, *Appl. Phys. Lett.* 67 (1995) 2925-2927.
- [45] S. Kopta, M. Salmeron, *J. Chem. Phys.* 113 (2000) 8249-8252.
- [46] J. Hu, X.-d. Xiao, D.F. Ogletree, M. Salmeron, *Surf. Sci.* 327 (1995) 358-370.
- [47] Y. Kuwahara, *Phys. Chem. Minerals* 24 (1999) 198-205.
- [48] Y. Kuwahara, *Phys. Chem. Minerals* 28 (2001) 1-8.
- [49] M. Baba, S. Kakitani, H. Ishii, T. Okuno, *Chem. Phys.* 221 (1997) 23-31.
- [50] T. Fukuma, Y. Ueda, S. Yoshioka, H. Asakawa, *Phys. Rev. Lett.* 104 (2010) 016101.
- [51] K. Miyata, K. Miyazawa, S.M.R. Akrami, T. Fukuma, *Jpn. J. Appl. Phys.* 54 (2015) 08LA03-1.
- [52] T. Fukuma, K. Kobayashi, K. Matsushige, H. Yamada, *Appl. Phys. Lett.* 87 (2005) 034101.
- [53] T. Fukuma, Y. Ueda, S. Yoshioka, H. Asakawa, *Phys. Rev. Lett.* 104 (2010).
- [54] S.-H. Loh, S.P. Jarvis, *Langmuir* 26 (2010) 9176-9178.
- [55] S.S. Lee, P. Fenter, K.L. Nagy, N.C. Sturchio, *Langmuir* 28 (2012) 8637-8650.
- [56] G.L. Gaines, *J. Phys. Chem.* 61 (1957) 1408-1413.
- [57] G.M. Bowers, D.L. Bish, R.J. Kirkpatrick, *Langmuir* 24 (2008) 10240-10244.
- [58] P.J. Sides, D. Faruqui, A.J. Gellman, *Langmuir* 25 (2009) 1475-1481.
- [59] L. Xu, M. Salmeron, *Langmuir* 14 (1998) 5841-5844.
- [60] P.M. Claesson, P. Herder, P. Stenius, J.C. Eriksson, R.M. Pashley, *J. Colloid Interface Sci.* 109 (1986) 31-39.
- [61] L. Xu, M. Salmeron, *Langmuir* 14 (1998) 2187-2190.
- [62] P.J. Scales, F. Grieser, T.W. Healy, *Langmuir* 6 (1990) 582-589.
- [63] R.M. Pashley, *J. Colloid Interface Sci.* 83 (1981) 531-546.
- [64] R.M. Pashley, *J. Colloid Interface Sci.* 80 (1981) 153-162.
- [65] R.S. Bradley, *Trans. Faraday. Soc.* (1939) 1361-1365.
- [66] H.G. Hansma, D.E. Laney, *Biophys. J.* 70 (1996) 1933-1939.
- [67] M.S. Metsik, *Soviet. Phys.: Solid State* 1 (1960) 991-997.
- [68] B.V. Deryagin, M.S. Metsik, *Soviet. Phys.: Solid State* 1 (1960) 1393-1399.
- [69] A.I. Bailey, *J. Appl. Phys.* 32 (1961) 1407-1412.
- [70] P.J. Bryant, L.H. Taylor, P.L. Gutshall, *Trans. Tenth Nat. Vacuum Symp., Macmillan and Co.*, 1963, 21-26.
- [71] A.I. Bailey, S.M. Kay, *Proc. R. Soc. (London) A* 301 (1967) 47-56.
- [72] M.S. Metsik, *J. Adhesion* 3 (1972) 307-314.
- [73] A.I. Bailey, H. Daniels, *J. Phys. Chem.* 77 (1973) 501-515.

- [74] K.-T. Wan, N. Aimard, S. Lathabai, R.G. Horn, B.R. Lawn, *J. Mater. Res.* 5 (1990) 172-182.
- [75] K.-T. Wan, B.R. Lawn, *Acta Metall. Mater.* 38 (1990) 2073-2083.
- [76] K.-T. Wan, D.T. Smith, B.R. Lawn, *J. Am. Ceram. Soc.* 75 (1992) 667-676.
- [77] P.L. Gutshall, J.M. Phillips, P.J. Bryant, G.M. Cole, *J. Vac. Sci. Technol.* 8 (1971) 85-87.
- [78] K. Müller, C.C. Chang, *Surf. Sci.* 14 (1969) 39-51.
- [79] K. Müller, C.C. Chang, *Surf. Sci.* 8 (1968) 455-458.
- [80] K.G. Bhattacharyya, *J. Electron. Spectrosc. Relat. Phenom.* 63 (1993) 289-306.
- [81] M.S. Metsik, L.M. Golub, *J. Appl. Phys.* 46 (1975) 1983-1986.
- [82] I.G. Higginbotham, R.H. Williams, A.J. McEvoy, *J. Phys. D: Appl. Phys.* 8 (1975) 1033-1043.
- [83] R.I. Revilla, Y.-L. Yang, C. Wang, *Surf. Interface Anal.* 47 (2015) 657-662.
- [84] P.A. Campbell, L.J. Sinnamon, C.E. Thompson, D.G. Walmsley, *Surf. Sci. Lett.* 410 (1998) L768-L772.
- [85] J.N. Israelachvili, D. Tabor, *Proc. R. Soc. (London) A* 331 (1972) 19-38.
- [86] J.N. Israelachvili, G.E. Adams, *J. Chem. Soc. Faraday Trans. 1* 74 (1978) 975-1001.
- [87] J. Klein, *J. Chem. Soc. Faraday Trans. 1* 79 (1983) 99-118.
- [88] J.L. Parker, H.K. Christenson, B.W. Ninham, *Rev. Sci. Instrum.* 60 (1989) 3135-3139.
- [89] H.K. Christenson, *Colloids Surf. A: Physicochem. Eng. Aspects* 123-124 (1997) 355-367.
- [90] H. Poppa, E.H. Lee, *Thin Solid Films* 32 (1976) 223-228.
- [91] H.K. Christenson, V.V. Yaminsky, *Coll. Surf. A: Physicochem. Eng. Asp.* 129 (1997) 67-74.
- [92] H.K. Christenson, P.M. Claesson, *Adv. Colloid Interface Sci.* 91 (2001) 391-436.
- [93] B.V. Derjaguin, *Kolloid Z.* 69 (1934) 155-164.
- [94] L.R. White, *J. Colloid Interface Sci.* 95 (1983) 286-287.
- [95] H.K. Christenson, *J. Phys. Chem.* 97 (1993) 12034-12041.
- [96] J.P. Quirk, R.M. Pashley, *J. Phys. Chem.* 95 (1991) 3300-3301.
- [97] P.M. McGuiggan, J.N. Israelachvili, *J. Mater. Res.* 5 (1990) 2232-2243.
- [98] B.V. Derjaguin, Z.M. Zorin, Y.I. Rabinovich, N.V. Churaev, *J. Colloid Interface Sci.* 46 (1974) 437-441.
- [99] A. Cherkin, *Nature* 305 (1983) 280.
- [100] V.V. Yaminsky, B.W. Ninham, R.M. Pashley, *Langmuir* 14 (1998) 3223-3235.
- [101] J. Middlehurst, L.R. Fisher, *Nature* 227 (1970).
- [102] J. Middlehurst, L.R. Fisher, *Nature (London)*, *Nature* 230 (1971) 575.
- [103] L.R. Fisher, J.N. Israelachvili, *J. Colloid Interface Sci.* 80 (1981) 528.
- [104] H.K. Christenson, V.V. Yaminsky, *Langmuir* 9 (1993) 2448-2454.
- [105] J.E. Curry, H.K. Christenson, *Langmuir* 12 (1996) 5729-5735.
- [106] M.M. Kohonen, H.K. Christenson, *Eur. Phys. J. E* 6 (2001) 315-323.
- [107] M.M. Kohonen, H.K. Christenson, *J. Phys. Chem. B* 106 (2002) 6685-6695.
- [108] T. Kovács, H.K. Christenson, *Faraday Discuss.* 159 (2012) 123-138.
- [109] T. Kovács, F.C. Meldrum, H.K. Christenson, *J. Phys. Chem. Lett.* 3 (2012) 1602-1606.
- [110] Y. Qiao, H.K. Christenson, *Phys. Rev. Lett.* 83 (1999) 1371-1374.
- [111] E.J. Wanless, H.K. Christenson, *J. Chem. Phys.* 101 (1994) 4260-4267.
- [112] L.R. Fisher, J.N. Israelachvili, *Colloids Surf.* 3 (1981) 303-319.
- [113] H.K. Christenson, *J. Colloid Interface Sci.* 121 (1988) 170-178.
- [114] H.K. Christenson, *J. Tribol.* 113 (1991) 224.

- [115] S. Ohnishi, A.M. Stewart, *Langmuir* 18 (2002) 6140-6146.
- [116] H.K. Christenson, *J. Colloid Interface Sci.* 104 (1985) 234-249.
- [117] R.G. Horn, J.N. Israelachvili, *J. Chem. Phys.* 75 (1980) 1400-1410.
- [118] H.K. Christenson, C.E. Blom, *J. Chem. Phys.* 86 (1987) 419-424.
- [119] H.K. Christenson, R.G. Horn, *Chem. Scr.* 25 (1985) 37-41.
- [120] H.K. Christenson, *Chem. Phys. Lett* 118 (1985) 455-458.
- [121] N. Maeda, H.K. Christenson, *Coll. Surf. A: Physicochem. Eng. Asp.* 159 (1999) 135-148.
- [122] H.K. Christenson, *Phys. Rev. Lett.* 73 (1994) 1821-1824.
- [123] M. Luna, J. Colchero, A.M. Baro, *Appl. Phys. Lett.* 72 (1998) 3461-3463.
- [124] H.K. Christenson, J. Fang, J.N. Israelachvili, *Phys. Rev. B* 39 (1989) 11750-11754.
- [125] H.K. Christenson, J.N. Israelachvili, *J. Colloid Interface Sci.* 117 (1987) 576-577.
- [126] S. Ohnishi, M. Hato, K. Tamada, H.K. Christenson, *Langmuir* 15 (1999) 3312-3316.
- [127] J. Schultz, K. Tsutsumi, J.-B. Donnet, *J. Colloid Interface Sci.* 59 (1977) 277-282.
- [128] K.L. Johnson, K. Kendall, A.D. Roberts, *Proc. R. Soc. (London) A* 324 (1971) 301-313.
- [129] H.K. Christenson, *Langmuir* 12 (1996) 1404-1405.
- [130] E.C.H. Silk, R.S. Barnes, *Philos. Mag.* 4 (1959) 970-972.
- [131] P. Frantz, M. Salmeron, *Tribol. Lett.* 5 (1998) 151-153.
- [132] M.M. Kohonen, H.K. Christenson, *Langmuir* 16 (2000) 7285-7288.
- [133] D. Nowak, H.K. Christenson, *Langmuir* 25 (2009) 9908-9912.
- [134] D. Nowak, M. Heuberger, M. Zäch, H.K. Christenson, *J. Chem. Phys.* 129 (2008) 154509.
- [135] H. Poppa, A.G. Elliot, *Surface Sci.* 24 (1971) 149-163.
- [136] M.G. Dowsett, R.M. King, E.H.C. Parker, *J. Vac. Sci. Technol.* 14 (1977) 711-717.
- [137] W.L. Baun, *Surf. Interface Anal.* 2 (1980) 145-147.
- [138] K.G. Bhattacharyya, *Langmuir* 5 (1989) 1155-1162.
- [139] S. Dorel, F. Pesty, P. Garoche, *Surf. Sci.* 446 (2000) 294-300.
- [140] R.K. Workmann, S. Manne, *Langmuir* 18 (2002) 661-666.
- [141] F. Ostendorf, C. Schmitz, S. Hirth, A. Kuhnle, J.J. Kolodziej, R. M, *Nanotechnology* 19 (2008) 305705.
- [142] F. Ostendorf, C. Schmitz, S. Hirth, A. Kuhnle, J.J. Kolodziej, R. M, *Langmuir* 25 (2009) 10764-10767.
- [143] D.A. Deshpande, K.R. Ghormare, N.D. Deshpande, A.V. Tankhiwale, *Thermochim. Acta* 66 (1983) 255-265.
- [144] B.M. Gatehouse, D.J. Lloyd, *J. Chem. Soc. Dalton Trans.* (1973) 70-72.
- [145] J.O. Thomas, R. Tellgren, I. Olovsson, *Acta Cryst. B*30 (1974) 1155-1166.
- [146] G.P. Vassilev, *Cryst. Res. Technol.* 31 (1996) 647-657.
- [147] F.D. Hunter, G.A. Jeffrey, *J. Chem. Phys.* 47 (1967) 3297-3302.
- [148] I. Leizerson, S.G. Lipson, *Langmuir* 20 (2004) 8423-8425.
- [149] S.G. Lipson, *Phase Transitions* 77 (2004) 677-688.
- [150] L. Xu, A. Lio, J. Hu, F.D. Ogletree, M. Salmeron, *J. Phys. Chem. B* 102 (1998) 540-548.
- [151] C.Y.K. Fung, R. Sedev, J.N. Connor, *Adv. Powder Technol.* 25 (2014) 1171-1176.
- [152] D. Beaglehole, H.K. Christenson, *J. Phys. Chem.* 96 (1992) 3395-3403.
- [153] D. Beaglehole, E.Z. Radlinska, B.W. Ninham, H.K. Christenson, *Phys. Rev. Lett.* 66 (1991) 2084-2087.
- [154] W. Cantrell, G.E. Ewing, *J. Phys. Chem. B* 105 (2001) 5434-5439.
- [155] G.E. Ewing, *Chem. Rev.* 106 (2006) 1511-1526.

- [156] T.E. Balmer, H.K. Christenson, N.D. Spencer, M. Heuberger, *Langmuir* 24 (2008) 1566-1569.
- [157] S. Ruthberg, L. Frenkel, *J. Res. Nat. Bureau of Standards* 68A (1964) 173-183.
- [158] L. Frenkel, *J. Res. Nat. Bureau of Standards* 68A (1964) 185-188.
- [159] N. Bano, A.K. Jonscher, *J. Mater. Sci.* 27 (1992) 1672-1682.
- [160] M.A. Chaudhry, *J. Mater. Sci.* 27 (1992) 5163-5168.
- [161] R. Guckenberger, M. Heim, G. Cevc, H.F. Knapp, W. Winegräbe, A. Hillebrand, *Science* 266 (1994) 1538-1540.
- [162] M. Heim, G. Cevc, R. Guckenberger, H.F. Knapp, W. Winegräbe, *Biophys. J.* 69 (1995) 489-497.
- [163] F.-R.F. Fan, A.J. Bard, *Proc. Natl. Acad. Sci. USA* 96 (1999) 14222-14227.
- [164] D. Beaglehole, *Physica A* 244 (1997) 40-44.
- [165] B.R. Rockland, *Anal. Chem.* 32 (1960) 1375-1376.
- [166] G. Rakhmatkariev, *Clays Clay Miner.* 54 (2006) 402-407.
- [167] L. Cheng, P. Fenter, K.L. Nagy, M.L. Schlegel, N.C. Sturchio, *Phys. Rev. Lett.* 87 (2001) 156103.
- [168] S.H. Park, G. Sposito, *Phys. Rev. Lett.* 89 (2002) 085501.
- [169] A. Meleshyn, *J. Phys. Chem. C* 112 (2008) 14495-14500.
- [170] A. Malani, K.G. Ayappa, *J. Phys. Chem. B* 113 (2009) 1058-1067.
- [171] A. Meleshyn, *Langmuir* 26 (2010) 13081-13085.
- [172] M. Odelius, M. Bernasconi, M. Parrinello, *Phys. Rev. Lett.* 78 (1997) 2855-2858.
- [173] P.J. Feibelman, *J. Chem. Phys.* 139 (2013) 074705.
- [174] J. Wang, A.G. Kalinichev, R.J. Kirkpatrick, R.T. Cygan, *J. Phys. Chem. B* 109 (2005) 15893-15905.
- [175] D.L. Sedin, K.L. Rowden, *Analytical Chemistry* 72 (2000) 2183-2189.
- [176] L. Zitzler, S. Herminghaus, F. Mugele, *Physical Review B* 66 (2002) 155436.
- [177] V. Barcons, A. Verdager, J. Font, M. Chiesa, S. Santos, *Journal of Physical Chemistry C* 116 (2012) 7757-7766.
- [178] Q. Zhong, D. Inniss, K. Kjoller, V.B. Elings, *Surface Science Letters* 290 (1993) L688-L692.
- [179] R. Garcia, A. San Paulo, *Phys. Rev. B* 60 (1999) 4961-4966.
- [180] A. San Paulo, R. Garcia, *Phys. Rev. B* 66 (2002) 041406.
- [181] S. Santos, A. Verdager, T. Souier, N.H. Thomson, M. Chiesa, *Nanotechnology* 22 (2011) 465705.
- [182] A. Verdager, S. Santos, G. Sauthier, J.J. Segura, M. Chiesa, J. Fraxedas, *Physical Chemistry Chemical Physics* 14 (2012) 16080-16087.
- [183] M. Köber, E. Sahagun, P. Garcia-Mochales, F. Briones, M. Luna, J.J. Saenz, *Small* 6 (2010) 2725-2730.
- [184] S. Santos, A. Verdager, M. Chiesa, *Journal of Chemical Physics* 137 (2012) 044201.
- [185] S. Santos, V. Barcons, H.K. Christenson, D.J. Billingsley, W.A. Bonass, J. Font, N.H. Thomson, *Appl. Phys. Lett.* 103 (2013) 063702.
- [186] J. Hu, X.-D. Xiao, D.F. Ogletree, M. Salmeron, *Science* 268 (1995) 267-269.
- [187] J. Hu, X.-D. Xiao, D.F. Ogletree, M. Salmeron, *Surf. Sci.* 344 (1995) 221-236.
- [188] J. Hu, X.-D. Xiao, M. Salmeron, *Appl. Phys. Lett.* 67 (1995) 476-478.
- [189] A. Verdager, G.M. Sacha, H. Bluhm, M. Salmeron, *Chem. Rev.* 106 (2006) 1478-1510.
- [190] F. Rieutord, M. Salmeron, *J. Phys. Chem. b* 102 (1998) 3941-3944.
- [191] L. Xu, M. Salmeron, *J. Phys. Chem. B* 102 (1998) 7210-7215.
- [192] P.B. Miranda, L. Xu, Y.R. Shen, M. Salmeron, *Phys. Rev. Lett.* 81 (1998) 5876-5879.

- [193] H. Bluhm, T. Inoue, M. Salmeron, *Surf. Sci. Lett.* 462 (2000) L599-L602.
- [194] O. Teschke, J.F. Valente, E.F. de Souza, *Chemical Physics Letters* 485 (2010) 133-136.
- [195] O. Teschke, J.F.V. Filho, E.F. de Souza, *Nanotechnology* 22 (2011) 165304.
- [196] D.W. Xu, K.M. Liechti, K. Ravi-Chandar, *Langmuir* 25 (2009) 12870-12873.
- [197] J.E. Sader, S.P. Jarvis, *Appl. Phys. Lett.* 84 (2004) 1801-1803.
- [198] A.J. Katan, M.H. van Es, T.H. Oosterkamp, *Nanotechnology* 20 (2009) 165703.
- [199] S. Santos, C.A. Amadei, A. Verdaguer, M. Chiesa, *J. Phys. Chem. C* 117 (2013) 10615-10622.
- [200] C.A. Amadei, S. Santos, S.O. Pehkonen, A. Verdaguer, M. Chiesa, *Journal of Physical Chemistry C* 117 (2013) 20819-20826.
- [201] C.A. Amadei, T.C. Tang, M. Chiesa, S. Santos, *J. Chem. Phys.* 139 (2013).
- [202] N.H. Thomson, S. Kasas, B.L. Smith, H.G. Hansma, P.K. Hansma, *Langmuir* 12 (1996) 5905-5908.
- [203] C. Rivetti, M. Guthold, C. Bustamante, *Journal of Molecular Biology* 264 (1996) 919-932.
- [204] O. Pietrement, D. Pastre, S. Fusil, J. Jeusset, M.-O. David, F. Landousy, L. Hamon, A. Zozime, E. Le Cam, *Langmuir* 19 (2003) 2536-2539.
- [205] D.J. Billingsley, A.J. Lee, N.A.B. Johansson, A. Walton, L. Stanger, N. Crampton, W.A. Bonass, N.H. Thomson, *Nanotechnology* 25 (2014) 025704.
- [206] D.J. Billingsley, J. Kirkham, W.A. Bonass, N.H. Thomson, *Physical Chemistry Chemical Physics* 12 (2010) 14727-14734.
- [207] T.C. Tang, C.A. Amadei, N.H. Thomson, M. Chiesa, *Journal of Physical Chemistry C* 118 (2014) 4695-4701.
- [208] S. Santos, V. Barcons, H.K. Christenson, J. Font, N.H. Thomson, *PLoS ONE* 6 (2011) e23821.
- [209] L.G. Schulz, *Acta Cryst.* 4 (1951) 483-486.
- [210] N.D. Lisgarten, *Trans. Faraday Soc.* 50 (1954) 684-690.
- [211] F.J. Lamelas, J.D. Schmidt, M. Xiong, *Phys. Rev. B* 58 (1998) 14270-14278.
- [212] G.F. Harrington, J.M. Campbell, H.K. Christenson, *Cryst. Growth Des.* 13 (2013) 5062-5067.
- [213] C.J. Stephens, Y. Mouhamad, F.C. Meldrum, H.K. Christenson, *Crystal Growth & Design* 10 (2010) 734-738.
- [214] J.M. Campbell, Ph. D. Thesis (2014) (available on request from <http://etheses.whiterose.ac.uk/6829/>).
- [215] M. Gillet, R. Delamare, E. Gillet, *J. Crystal Growth* 279 (2005) 93-99.
- [216] R. Delamare, M. Gillet, E. Gillet, P. Guaino, *Surf. Sci.* 601 (2007) 2675-2679.
- [217] I. Matolinova, M. Gillet, E. Gillet, V. Matolin, *Nanotechnology* 20 (2009) 445604.
- [218] M. Akai-Kasaya, C. Ohmori, T. Kawanishi, M. Nashiki, A. Saito, M. Aono, Y. Kuwahara, *Nanotechnology* 21 (2010) 365601.
- [219] P. Putsche, L. Tumbek, A. Winkler, *J. Chem. Phys.* 137 (2012) 134701.
- [220] F.A. Koch, R.W. Vook, *Thin Solid Films* 14 (1972) 231-248.
- [221] H. Li, et al., *J. Phys. Chem. B* 113 (2009) 8795-8799.
- [222] L. Bertsch, H.W. Habgood, *J. Phys. Chem.* 67 (1963) 1621-1628.
- [223] D. Bonenfant, M. Kharoune, P. Niquette, M. Mimeault, R. Hausler, *Sci. Technol. Adv. Mater.* 9 (2008) 013007.
- [224] Y. Wang, M.D. LeVan, *J. Chem. Eng. Data* 55 (2010) 3189-3195.
- [225] S.U. Rege, R.T. Yang, *Chem. Eng. Sci.* 56 (2001) 3781-3796.
- [226] G.D. Pirngruber, P. Raybaud, Y. Belmabkhout, J. Čejka, A. Zúkal, *Phys. Chem. Chem. Phys.* 12 (2010) 13534-13546.

- [227] R.W. Stevens, R.V. Siriwardane, J. Logan, *Energy & Fuels* 22 (2008) 3070-3079.
- [228] P. Galhotra, J.G. Navea, S.C. Larsen, V.H. Grassian, *Energy Environ. Sci.* 2 (2009) 401-409.
- [229] A. Zúkal, A. Mayerová, J. Čejka, *Phys. Chem. Chem. Phys.* 12 (2010) 5240–5247.
- [230] J. Kanellopoulos, C. Gottert, D. Schneider, B. Knorr, D. Prager, H. Ernst, F. D., *J. Catal.* 255 (2008) 68-78.
- [231] C. Morterra, A. Zecchina, S. Coluccia, A. Chiorino, *J. Chem. Soc. Faraday Trans. 1* 73 (1977) 1544-1559.
- [232] J. Baltrusaitis, V.H. Grassian, *J. Phys. Chem. B* 109 (2005) 12227-12230.
- [233] Y. Lykhach, T. Staudt, R. Streber, M.P.A. Lorenz, A. Bayer, H.-P. Steinrück, J. Libuda, *Eur. Phys. J. B.* 75 (2010) 89-100.
- [234] W. Bak, B. Sung, J. Kim, S. Kwon, B. Kim, W. Jhe, *Appl. Phys. Lett.* 106 (2015) 013102.
- [235] R.D. Piner, C.A. Mirkin, *Langmuir* 13 (1997) 6864–6868.
- [236] Z.G. Liu, Z. Li, H.L. Zhou, G. Wei, Y.H. Song, L. Wang, *Micron* 36 (2005) 525-531.
- [237] C. Spagnoli, K. Loos, A. Ulman, M.K. Cowman, *J. Am. Chem. Soc.* 125 (2003) 7124-7128.
- [238] W. Chen, A.S. Foster, M.J. Alava, L. Laurson, *Phys. Rev. Lett.* 114 (2015) 095502.
- [239] H. Li, X.C. Zeng, *J. Chem. Theory Comput.* 8 (2012) 3034-3043.
- [240] Q. Li, J. Song, F. Besenbacher, M. Dong, *Acc. Chem. Res.* 48 (2014) 119-127.
- [241] M. Cheng, et al., *ACS Nano* 8 (2014) 3955-3960.

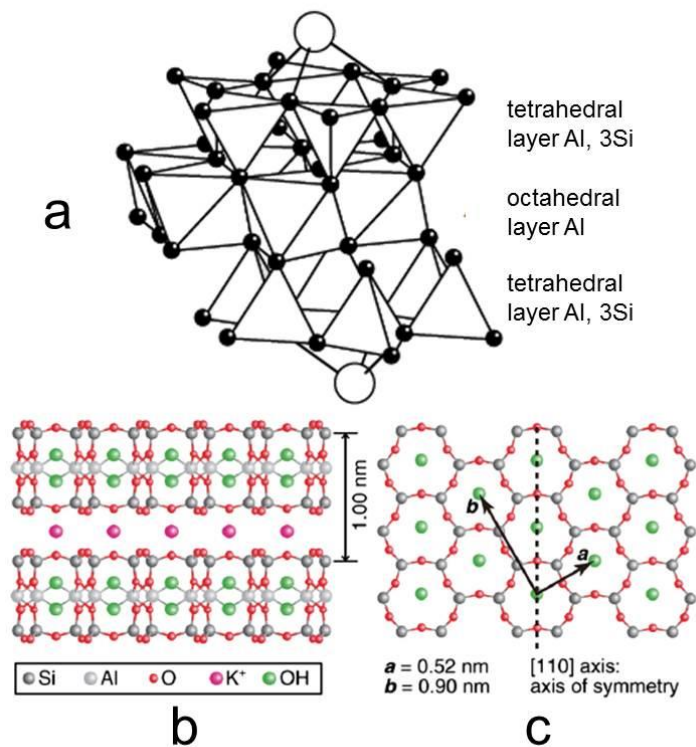


Figure 1 (a) Idealised structure of muscovite mica with two tetrahedral layers of SiO₄ above and below an octahedral layer of AlO₆. One in four Si in the tetrahedral layers is randomly substituted for Al and the resultant negative charge is neutralised by the K⁺ between the centres of hexagonal SiO₄ rings in opposing tetrahedral layers. (b) [110] projection, showing the hydroxyl groups in the octahedral layers that are not shared with the tetrahedral layers. (c) The basal plane [001] of the cleaved surface showing the ditrigonal symmetry of the oxygen hexagons, the *a* and *b* vectors of the unit cell, and the [110] symmetry axis.

Adapted from L. Cheng, P. Fenter, K.L. Nagy, M.L. Schlegel, N.C. Sturchio, Phys. Rev. Lett. 87 (2001) 156103 (a) and T. Fukuma, Y. Ueda, S. Yoshioka, H. Asakawa, Phys. Rev. Lett. 104 (2010) 016101 (b,c).

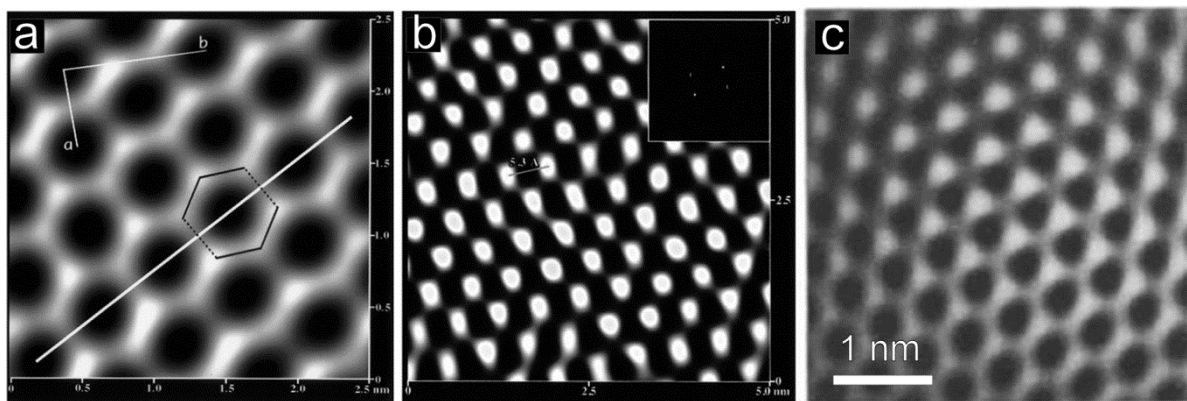


Figure 2 Examples of the two types of AFM image of the mica surface. a) Hexagonal rings of SiO₄ tetrahedra; b) Hexagonal array of bright spots with periodicity of 0.53nm. a) and b) reprinted with permission from Kuwahara (Phys Chem Minerals 26 (1999) 198-205. c) Example of the two types of mica lattice acquired in a single AFM image, demonstrating the importance of the tip-sample interaction on the observed surface topography. Reprinted with permission from Coleman et al. Surf Sci 297 (1993) 359-370.

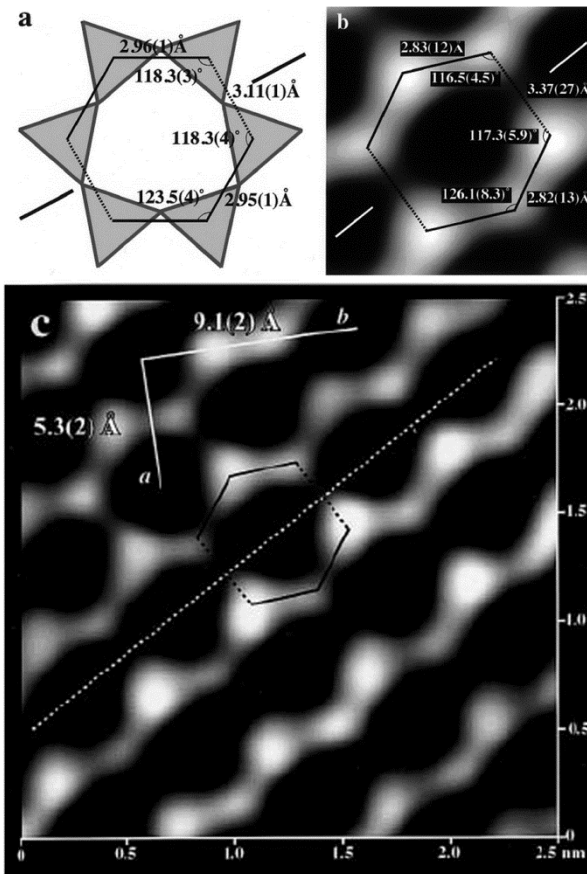


Figure 3 The ditrigonal symmetry of the mica lattice taken using contact mode AFM under water. a) and b) Reprinted with permission from Fig. 5 of Kuwahara, Phys Chem Minerals 26 (1999) 198-205. c) Reprinted with permission from Fig. 2c of Kuwahara, Phys Chem Minerals 28 (2001) 1-8.

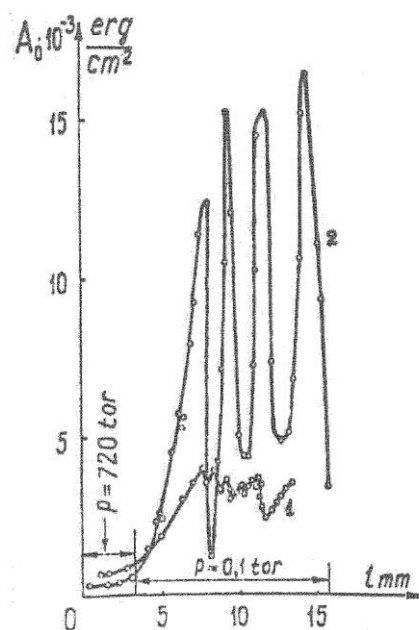


Figure 4 Work of cleavage as a function of depth of cleavage in mm for mica crystal in a vacuum of 10^{-1} mm Hg (1 torr) - after an initial 3 mm of cleavage at 720 torr. $1 \text{ erg/cm}^2 = 1 \text{ mJ/m}^2$. Note the dramatic rise in the work as the charge on the surfaces increases during cleavage at a speed of 0.5 mm s^{-1} (curve 2), and the fall as a discharge occurs, and how this variation is significantly smaller for a slower cleavage speed of 0.05 mm s^{-1} (curve 1).

Reprinted with permission from M.S. Metsik, J. Adhesion 3 (1972) 307-314.

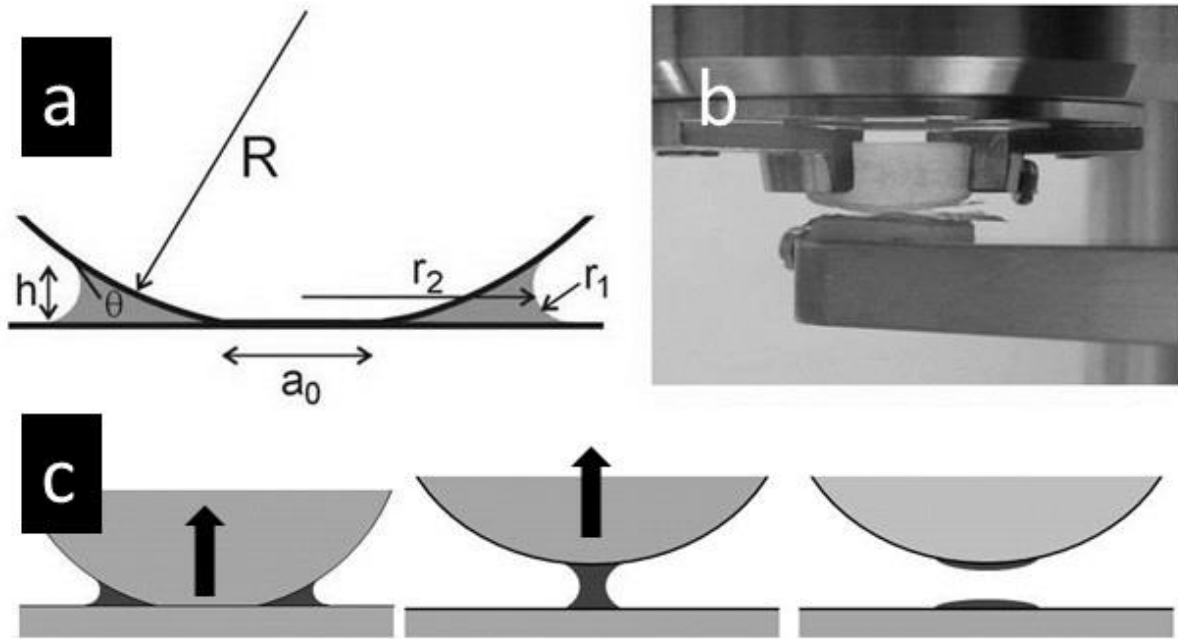


Figure 5 (a) Cross-section through surfaces parallel to one cylinder axis, (b) actual surface configuration during capillary-condensation experiment in the SFA. From T. Kovács, T., H. K. Christenson, *Faraday Discuss.* (2012) 159, 123-138 (Reproduced by permission of The Royal Society of Chemistry).

(c) The annular condensate around contact of surfaces becomes a bridge of liquid on separation of the surfaces and the bridge then evaporates and snaps, turning into two droplets on the opposing surfaces.

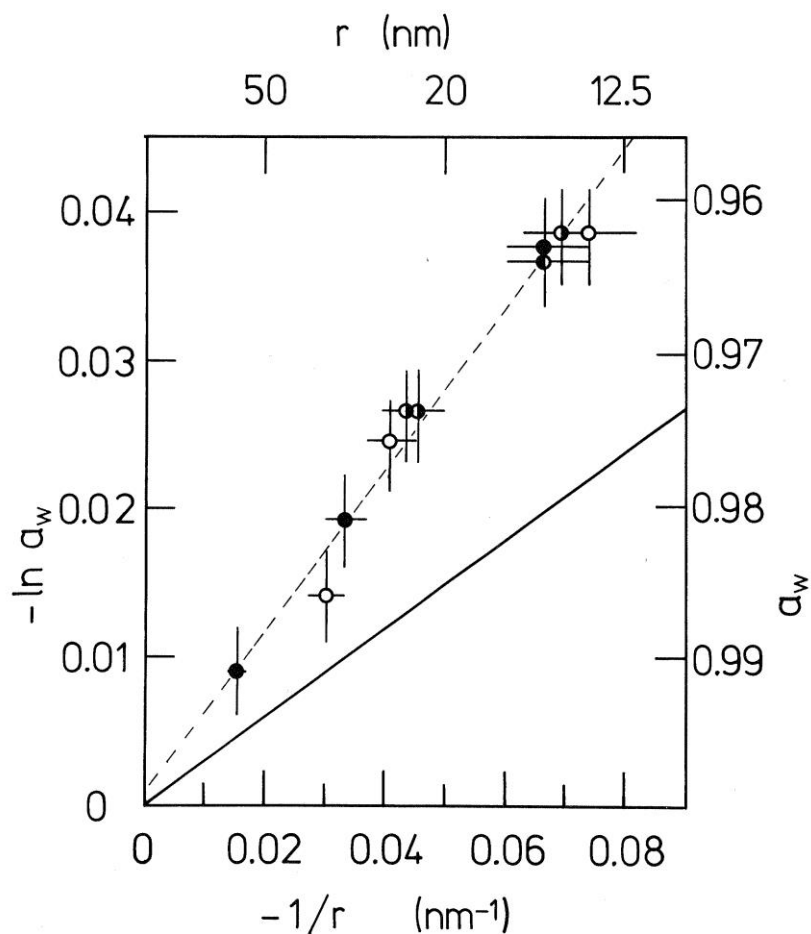


Figure 6 The natural logarithm of the water activity (= fractional degree of saturation) as a function of the inverse radius of the condensate-liquid interface, for water condensing from the nonpolar liquid octamethylcyclotetrasiloxane, around the contact point of two crossed cylinders of mica. The different points are from separate series of measurements with different mica surfaces. The solid line is the prediction of a modified Kelvin equation (eq. 1), and the dashed line is a least-squares fit to the data.

Reprinted with permission from H.K. Christenson, *J. Colloid Interface Sci.* 104 (1985) 234.

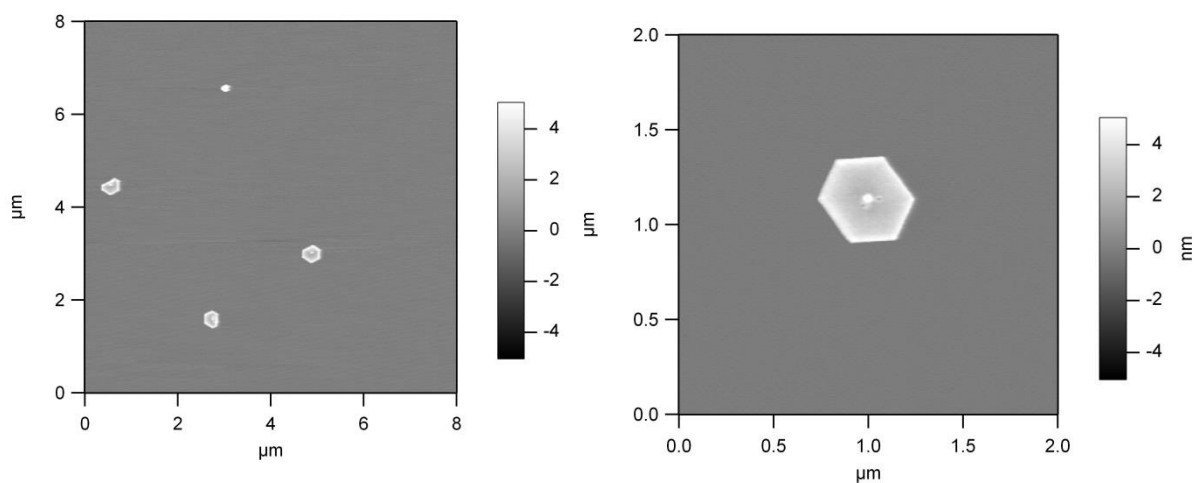


Figure 7 AFM tapping mode images of crystallites on air-cleaved mica surface after drying over P_2O_5 , showing the hexagonal symmetry that is most likely caused by the pseudohexagonal/ditrigonal symmetry of the mica basal plane. Images by N. Maeda and M. Kohonen.

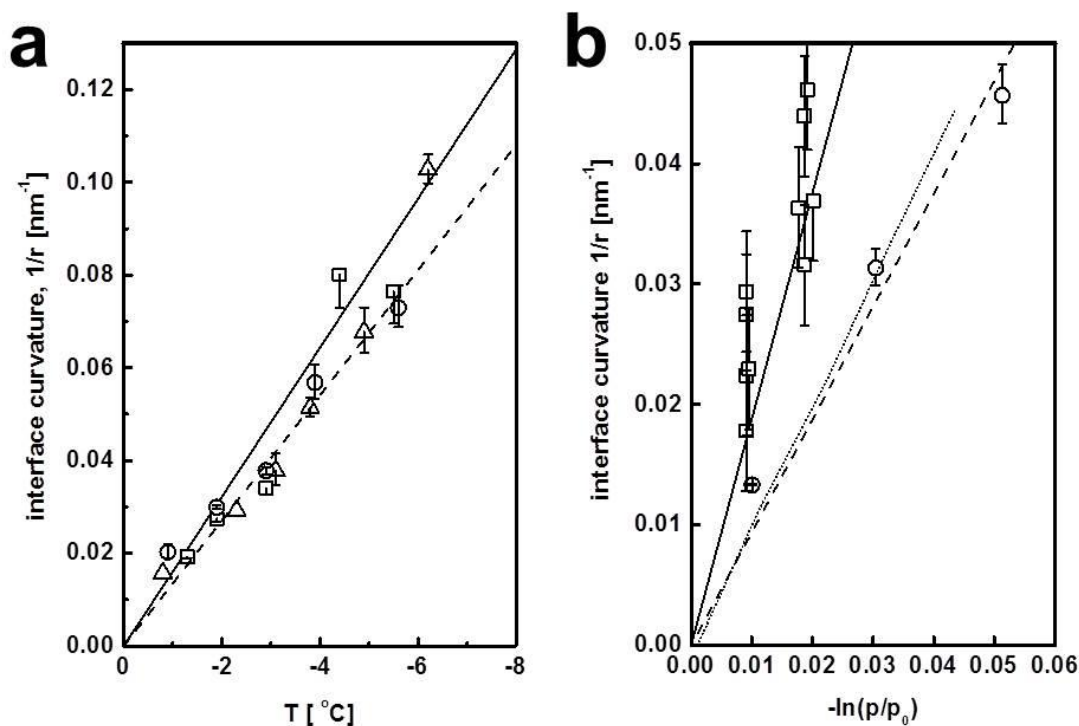


Figure 8 – Interfacial curvature of water condensates between mica surfaces below zero (a) and at room temperature (b). The symbols in (a) are the results of 3 separate series of measurements with different mica surfaces and the solid line is the prediction of the modified Gibbs-Thomson eq (eq. 5). The dashed line is the predicted result if the condensates contain dissolved K_2CO_3 from all K^+ on the mica surfaces in contact with the condensate.

The open squares in (b) are the results with hydrogen mica at room temperature, and the solid line is the prediction of the Kelvin eq (eq. 1). The open circles are the results with potassium mica at room temperature and the dashed line is a least squares fit to these points. The dotted line is a rescaling of the fit to the experimental points of Figure 6 to take into account the difference between the surface tension of water and the interfacial tension between OMCTS and water. The agreement between the dotted and the dashed line shows that there are similar concentrations of K_2CO_3 in the water condensing from vapour and from OMCTS.

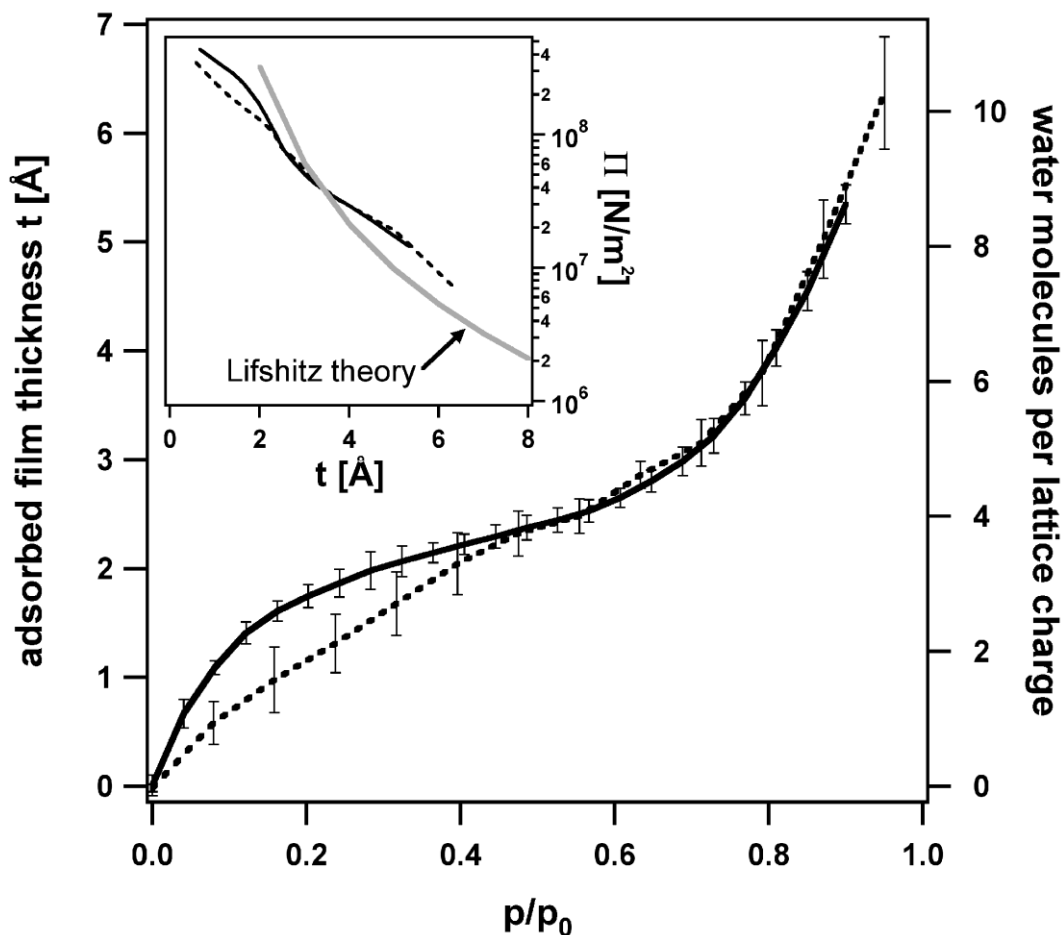


Figure 9 Water vapour adsorption isotherms measured on hydrogen mica (dashed line) and potassium mica (solid line) at 22.7 °C in terms of mean water layer thickness (left) or average number of water molecules per lattice charge, or K^+ for freshly cleaved mica. Note the significant reduction in the knee of the adsorption term at low p/p_0 values on replacement of the K^+ with H^+ ., but the experimentally insignificant change $p/p_0 > 0.5$. The inset shows The repulsive van der Waals force between the mica and the vapour-water interface calculated from the adsorption isotherms is shown in the inset for K^+ -mica (solid line) and H^+ -mica (dashed line).The gray line shows the predictions of the Lifshitz theory.

Reprinted with permission from T.E. Balmer, H.K. Christenson, N.D. Spencer, M.

Heuberger, Langmuir 24 (2008) 1566-69, Copyright 2008, American Chemical Society.

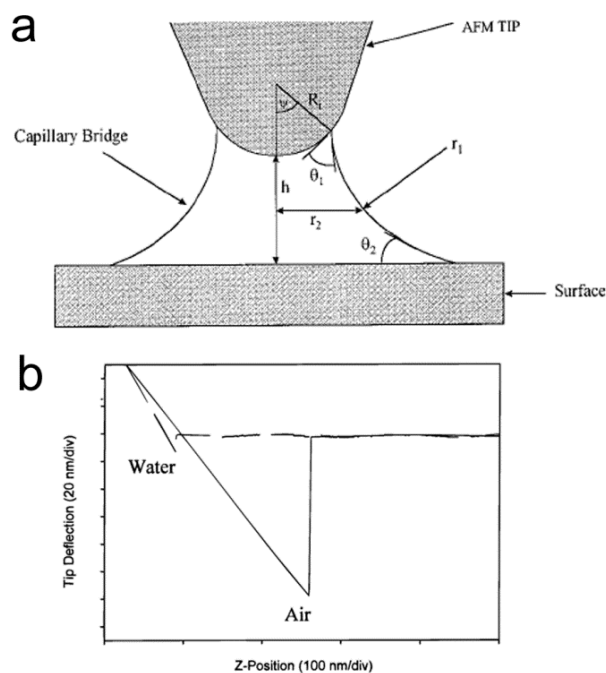


Figure 10 a) Schematic representation of a liquid capillary bridge between an AFM tip and a surface: r_1 and r_2 are principle radii of curvature of the liquid bridge; R_t is the radius of curvature of the AFM tip; θ_1 and θ_2 are contact angles with the tip and surface respectively. b) A comparison of force curves in water and ambient air environments demonstrating the large adhesive force cause by the capillary bridge in air. Tip deflection corresponds to the force on the AFM cantilever. The capillary interaction causes 120nm of negative deflection of the cantilever towards the mica surface, which for the nominal spring constants of the cantilevers used here ($0.1\text{-}0.4 \text{ Nm}^{-1}$), puts the capillary force in the range 12-48 nN. a) Fig. 1 and b) Fig. 2 reprinted with permission from Sedin and Rowlen, *Anal Chem*, 72 (2000) 2183-2189, Copyright 2000, American Chemical Society.

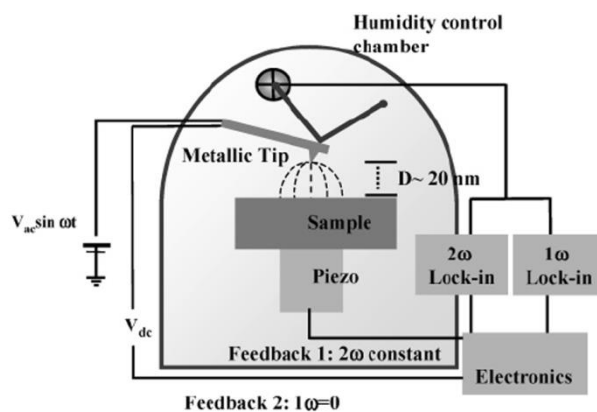


Figure 11 Schematic of a scanning polarisation force microscopy (SPFM) set-up. A few volts DC are applied to the conducting cantilever and tip to produce the electric field. A frequency dependent AC voltage is used to induce the polarisation signal of the dielectric between the tip and surface. A combination of demodulation and two feedback loops are used to separate the surface topography and contact potential contributions. Reprinted with permission from Fig. 17 in Verdaguer *et al.*, Chem Rev. 106 (2006) 1478-1510, Copyright 2006, American Chemical Society.

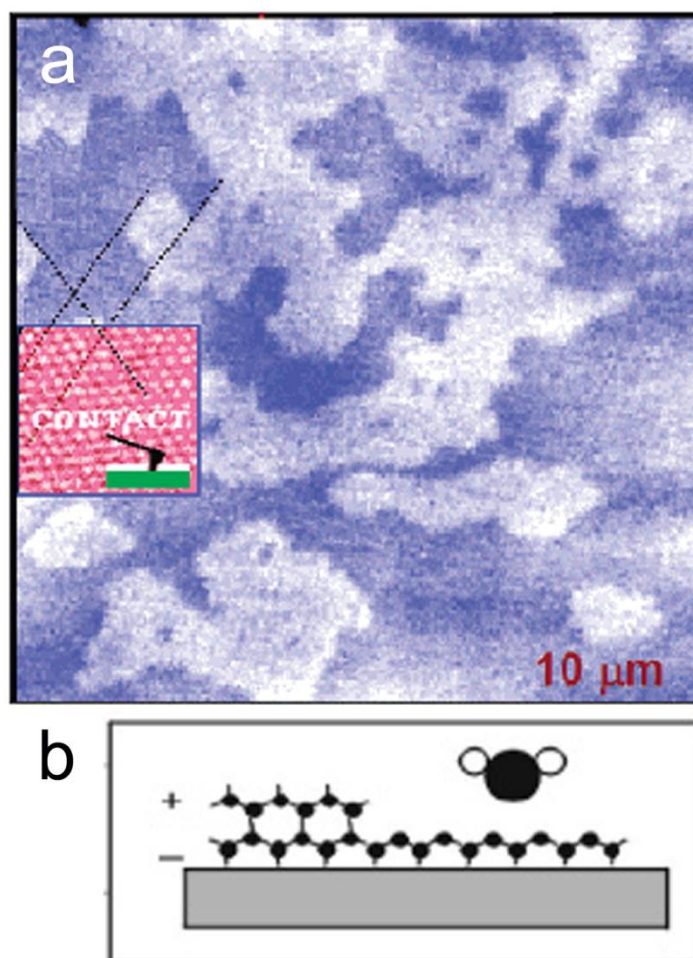


Figure 12: a) Example of SPFM image showing two phases of water on mica where the higher one (proposed as phase II) shows evidence of hexagonal symmetry. b) Proposed ice-like bilayer structure of water on mica from sum-frequency generation (Bluhm et al., 2000) and SPFM. Reprinted with permission from Figs. 18 and 20 in Verdaguer *et al.*, Chem Rev. 106 (2006) 1478-1510, Copyright 2006, American Chemical Society.

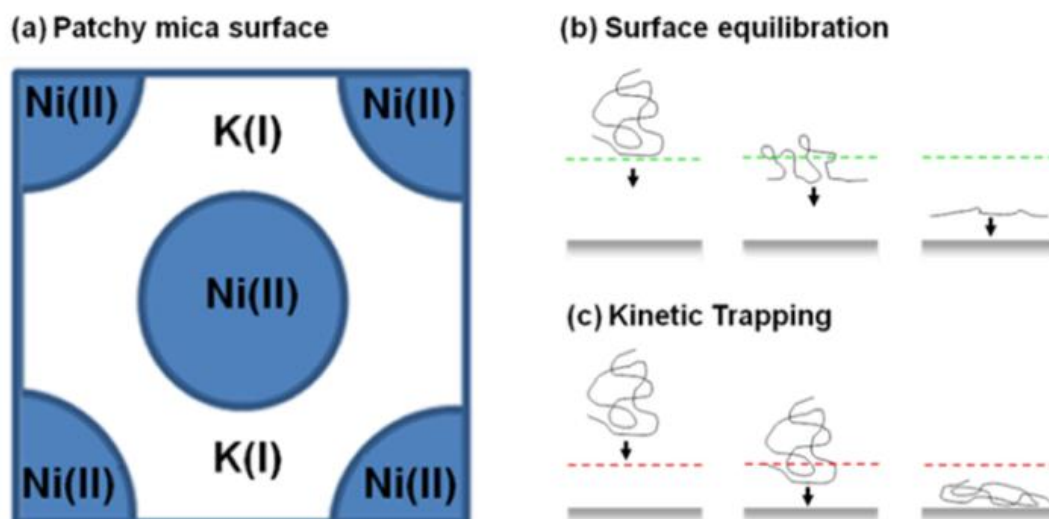


Figure 13 a) Schematic representation of an idealised patchy Ni-mica surface where 50% of the surface has been ion-exchanged with Ni and the other 50% remains as either K-mica, H-mica or Mg-mica, the exact composition of which should depend on the buffer conditions under which DNA is deposited onto the surface. b) and c) are schematic representations of linear DNA molecules adsorbing to the mica surface, showing how the final surface conformation will depend on both the trajectory from bulk solution and both the composition of the mica surface and the bulk solution. b) Represents surface equilibration where long range forces dominate and c) represents kinetic trapping where short range forces dominate. Reprinted with permission from Fig. 2 in Billingsley et al. *Nanotechnology* 25 (2014) 025704.

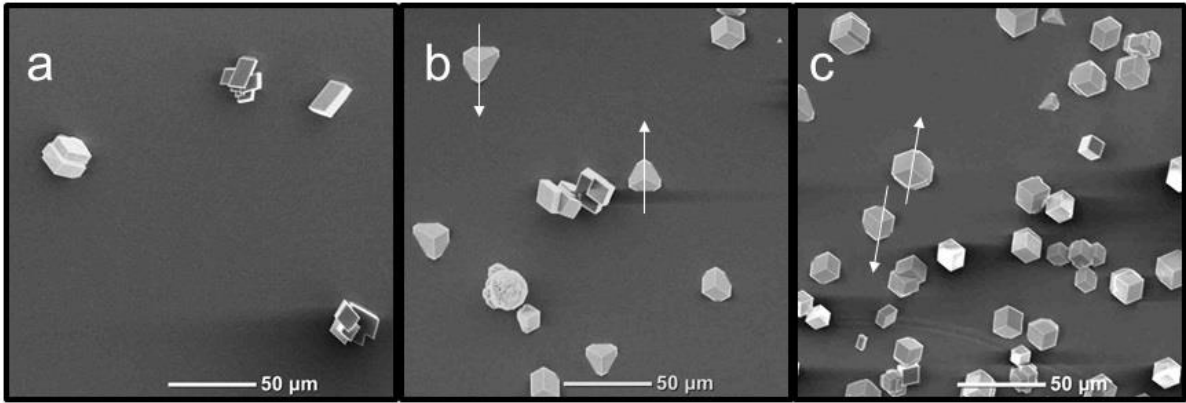


Figure 14 Scanning electron microscopy images of calcite precipitated on mica surfaces from a metastable solution of 5 mM CaCl_2 and 5mM Na_2CO_3 after 2h. Left-hand image shows unoriented crystals on freshly cleaved mica, the centre image shows more oriented crystals on mica weathered for 1 hour in laboratory air at a humidity of ca. 40% before precipitation, and right-hand image has almost all calcite crystals oriented after 12 h of weathering time before precipitation. Note the two orientations of the calcite crystals 180° apart, indicated by the arrows. Images by Dominika Nowak.

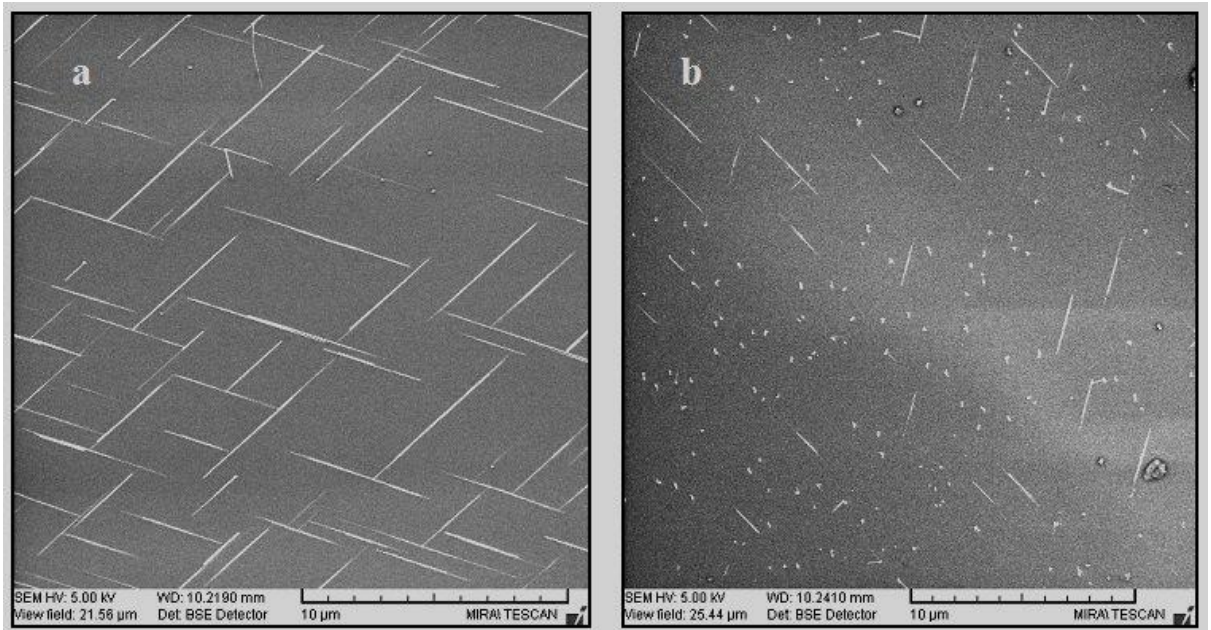


Figure 15 SEM images (back-scattered electron mode) of WO_3 nanowires grown on two ‘face-to-face’ mica cleavage planes (a and b). The orientation and length of the WO_3 nanowires are sensitive to the amount of K on the surface, so the large difference between the images shows that there can be a significant asymmetry in the K distribution on cleavage.

From I. Matolinova, M. Gillet, E. Gillet, V. Matolin, *Nanotechnology* 20 (2009) 445604.